Volume 2 ▪ Issue 2 ▪ May 2011

INTERNATIONAL JOURNAL OF

ROBOTICS AND AUTOMATION (IJRA)

ISSN : 2180-1312
Publication Frequency: 6 Issues / Year

CSC PUBLISHERS
http://www.cscjournals.org

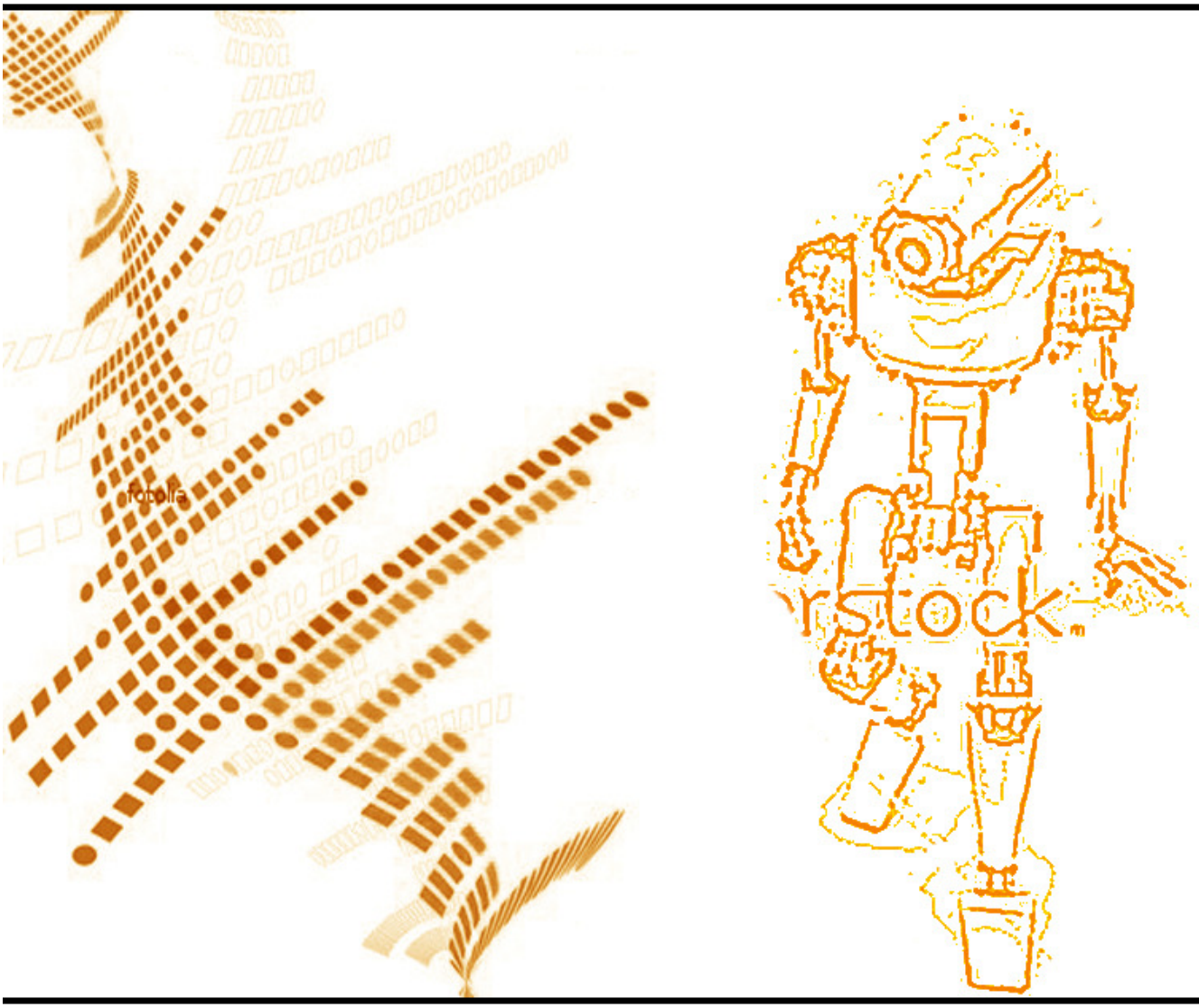

INTERNATIONAL JOURNAL OF ROBOTICS AND AUTOMATION (IJRA)

VOLUME 2, ISSUE 2, 2011

EDITED BY
DR. NABEEL TAHIR

ISSN (Online): 2180-1312

I International Journal of Robotics and Automation (IJRA) is published both in traditional paper form and in Internet. This journal is published at the website http://www.cscjournals.org, maintained by Computer Science Journals (CSC Journals), Malaysia.

IJRA Journal is a part of CSC Publishers
Computer Science Journals
http://www.cscjournals.org

INTERNATIONAL JOURNAL OF ROBOTICS AND AUTOMATION (IJRA)

Book: Volume 2, Issue 2, May 2011
Publishing Date: 31-05-2011
ISSN (Online): 2180-1312

IJRA Journal is a part of CSC Publishers
http://www.cscjournals.org

Published in Malaysia

Typesetting: Camera-ready by author, data conversation by CSC Publishing Services – CSC Journals, Malaysia

CSC Publishers, 2011

EDITORIAL PREFACE

Robots are becoming part of people's everyday social lives - and will increasingly become so. In future years, robots may become caretaking assistants for the elderly or academic tutors for our children, or medical assistants, day care assistants, or psychological counselors. Robots may become our co-workers in factories and offices, or maids in our homes. It is the fourth issue of volume first of International Journal of Robotics and Automation (IJRA). IJRA published six times in a year and it is being peer reviewed to very high International standards.
.

The initial efforts helped to shape the editorial policy and to sharpen the focus of the journal. Starting with volume 2, 2011, IJRA appears in more focused issues. Besides normal publications, IJRA intend to organized special issues on more focused topics. Each special issue will have a designated editor (editors) – either member of the editorial board or another recognized specialist in the respective field.

IJRA looks to the different aspects like sensors in robot, control systems, manipulators, power supplies and software. IJRA is aiming to push the frontier of robotics into a new dimension, in which motion and intelligence play equally important roles. IJRA scope includes systems, dynamics, control, simulation, automation engineering, robotics programming, software and hardware designing for robots, artificial intelligence in robotics and automation, industrial robots, automation, manufacturing, and social implications etc. IJRA cover the all aspect relating to the robots and automation.

The IJRA is a refereed journal aims in providing a platform to researchers, scientists, engineers and practitioners throughout the world to publish the latest achievement, future challenges and exciting applications of intelligent and autonomous robots. IJRA open access publications has greatly speeded the pace of development in the robotics and automation field. IJRA objective is to publish articles that are not only technically proficient but also contains state of the art ideas and problems for international readership.

In order to position IJRA as one of the top International journal in signal processing, a group of highly valuable and senior International scholars are serving its Editorial Board who ensures that each issue must publish qualitative research articles from International research communities relevant to signal processing fields.

IJRA editors understand that how much it is important for authors and researchers to have their work published with a minimum delay after submission of their papers. They also strongly believe that the direct communication between the editors and authors are important for the welfare, quality and wellbeing of the Journal and its readers. Therefore, all activities from paper submission to paper publication are controlled through electronic systems that include electronic submission, editorial panel and review system that ensures rapid decision with least delays in the publication processes.

To build its international reputation, we are disseminating the publication information through Google Books, Google Scholar, Directory of Open Access Journals (DOAJ), Open J Gate, ScientificCommons, Docstoc and many more. Our International Editors are working on establishing ISI listing and a good impact factor for IJRA. We would like to remind you that the success of our journal depends directly on the number of quality articles submitted for review. Accordingly, we would like to request your participation by submitting quality manuscripts for review and encouraging your colleagues to submit quality manuscripts for review. One of the great benefits we can provide to our prospective authors is the mentoring nature of our review process. IJRA provides authors with high quality, helpful reviews that are shaped to assist authors in improving their manuscripts.

Editorial Board Members
International Journal of Robotics and Automation (IJRA)

TABLE OF CONTENTS

Volume 2, Issue 2, May 2011

Pages

V/*F* Control of Squirrel Cage Induction Motor Drives Without Flux or Torque Measurement Dependency

Walid Emar *walidemar@yahoo.com*
Electrical Engineering Department
Isra University
11622 Amman, Jordan

Hussein Sarhan *hussein_52@hotmail.com*
Mechatronics Engineering Department
Balqa' Applied University
Amman, Jordan

Rateb Al-Issa *ratebissa@yahoo.com*
Mechatronics Engineering Department
Balqa' Applied University
Amman, Jordan

Issam TTrad *Issam_161@yahoo.com*
Faculty of science and information
Jadara University
Irbid, Jordan

Mahmoud Awad *Dr_Awad_M@yahoo.com*
Electrical Engineering Department
Balqa' Applied University
Amman, Jordan

Abstract

Based on the popular constant volts per hertz principle, two improvement techniques are presented: keeping maximum torque constant or keeping magnetic flux constant. An open-loop inverter-three-phase squirrel-cage induction motor drive system that provides constant maximum torque or increased maximum torque and reduced slip speed at frequencies below the nominal frequency has been modeled, simulated and tested. Load performance analysis of the proposed system under different operation conditions was provided. These principles of operation are extended to the case of operation from variable frequency or variable voltage control method. Finally, the effects of the non-sinusoidal voltage and/or current wave shapes are covered.

The results show that both suggested improvement techniques (constant torque or constant flux) improve the steady-state performance A.C. drive system with squirrel cage induction motors. The slip speed has been decreased and the starting torque and maximum torque have been increased, which means that the suggested control techniques can be used in drive systems with short time operating mode under light loads.

Keywords: Induction Motor Drive, Constant Volts Per Hertz, Torque Speed Curve, dq Transformation, State-space Model.

Nomenclature:

v_{ds} = d-axis component of the stator voltage, V

v_{qs} = q-axis component of the stator voltage, V

i_{ds} = d-axis component of the stator current, A

i_{qs} = q-axis component of the stator current, A

i'_{dr} = d-axis component of the rotor current referred to the stator, A

i'_{qr} = q-axis component of the rotor current referred to the stator, A

V or V_s = stator voltage effective value

L_s = stator inductance, H

L'_r = rotor inductance referred to the stator, H

L_m = mutual inductance between rotor and stator, H

$L_{ss} = L_s + L_m$, H

$L'_{rr} = L'_r + L_m$, H

ω_s = stator electrical angular speed, rad/s

ω_r = rotor electrical angular speed, rad/s

$\omega_m = \frac{2}{P}\omega_r$, rotor mechanical angular speed, rad/s

P = number of poles

T_e = electromagnetic developed torque, N.m

T_m = load torque, N.m

J = equivalent moment of inertia, kg.m^2

1. INTRODUCTION

The three-phase squirrel cage induction motor is the most widely used motor type in the industry because of its good self-starting capability, simple and rugged structure, low cost and reliability [1-5]. In spite of this popularity, the induction motor has two basic limitations: (1) The standard motor is not a true constant-speed machine, its full-load slip varies from less than 1% (in high-horsepower motors) to more than 5% (in fractional-horsepower motors), and (2) It is not inherently capable of providing variable-speed operation [2,3]. Both of these limitations require consideration to meet quality and accuracy requirements of induction motor drive applications.

The limitations of induction motor can be solved through the use of adjustable speed control based on pulse width modulation techniques [4]. The basic control action involved in adjustable speed control of induction motors is to apply a variable frequency variable magnitude AC voltage to the motor to achieve the aims of variable speed operation [5]. Voltage source inverters and current source inverters are used in adjustable speed AC drives. However, voltage source inverters with constant Volts/Hertz (*V/f*) are more popular, especially for applications without position control requirements, or where the need for high accuracy of speed control is not crucial.

Ideally, by keeping a constant *V/f* ratio for all frequencies the torque-speed curve of induction motor can be reproduced at any frequency. In this case, the stator flux, stator current, and torque will be constant at any frequency [6]. The great majority of variable-speed drives in operation today are of this type although almost all research has been concentrated in field-oriented control theory, and little has been published about constant *V/f* operation. Its practical application at low frequency is still challenging, due to the influence of the stator resistance and the necessary rotor slip to produce torque [7].

In addition, the nonlinear behavior of the pulse-width modulated voltage-source inverter in the low voltage range makes it difficult to use constant *V/f* drives at frequencies below 3Hz [8, 9]. The performance of induction motor operating at constant *V/f* ratio can be improved by using different techniques, such as stator resistance compensation, slip compensation and vector compensation. The stator resistance compensation method consists of boosting the stator voltage by the magnitude of the current-resistance drop. Slip compensation results in increasing the operating frequency (speed). Vector compensation requires measurement of both voltage and current and accurate knowledge of machine inductances [10].

In this paper, two techniques to improve the performance of the inverter-induction motor drive system with constant *V/f* ratio controller are presented. The first technique is based on keeping the maximum torque constant for all operating frequencies, and equals to its value at nominal frequency. The second technique is based on maintaining the magnetic flux constant at all operating frequencies and equals to its nominal value. The proposed techniques are validated by simulation and experimental results. It is shown that large load torques are obtained, even in the low frequency range, with significantly reduced steady-state error in speed.

These principles of operation are extended to the case of operation from variable frequency and/or variable voltage control method. Finally, the effects of the non-sinusoidal voltage and/or current wave shapes are covered.

2. MODELING SYSTEM COMPONENTS

The block diagram of inverter-three-phase squirrel cage induction motor drive system is presented in figure 1. It consists of IGBT-inverter-based AC to AC converter, three-phase squirrel cage induction motor and controller. In order to analyze the system performance, all of these components should be modeled (mathematically described).

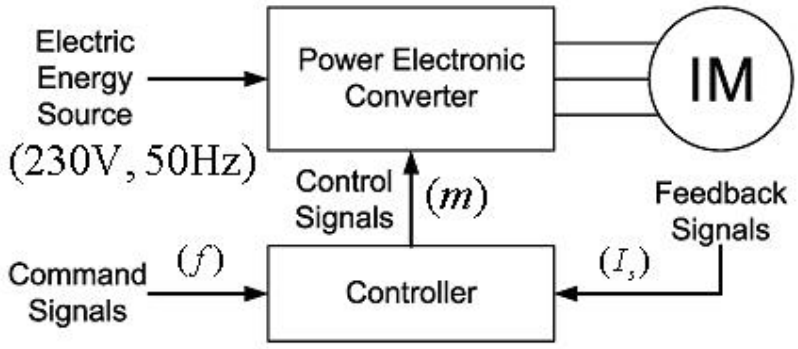

FIGURE 1: Block diagram of inverter-three phase squirrel-cage induction motor drive system

2.1. Modeling of the IGBT-Inverter-Based AC to AC Converter

The frequency converter is considered to be an ideal system, where the voltage at the dc side of the converter has no AC component. For sinusoidal pulse width modulation SPWM, the ratio of the amplitude of the sinusoidal waveform to the amplitude of the triangular waveform is called the modulation index *m*, which can be in the range of 0 to 1 [11]. The stator voltage V_s can be defined as:

$$V_s = m\, V_n \quad (1)$$

Where:

V_n = nominal value of stator voltage.

The frequency of the stator voltage *f* equals the frequency of the sinusoidal input waveform f_{in}.

$$f = f_{in} \quad (2)$$

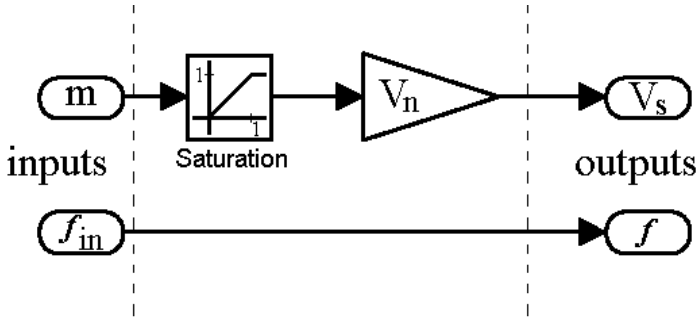

FIGURE 2: Steady-state model of inverter.

Varying the modulation index and the sinusoidal waveform frequency will change the RMS value of the stator voltage and frequency. Eqs. 1 and 2 constitute the steady-state model of inverter, shown in figure 2.

2.2. Modeling of Controller and Control Circuits

Based on the principle of *V/f* = constant, the controller must apply the following function:

$$m = \begin{cases} Kf, 0 < f < f_n \\ 1, \quad f \geq f_n \end{cases} \tag{3}$$

Where:

$K = 1/f_n$, and f_n = nominal frequency (50Hz). The block diagram of *V/f* = constant controller is shown in figure 3.

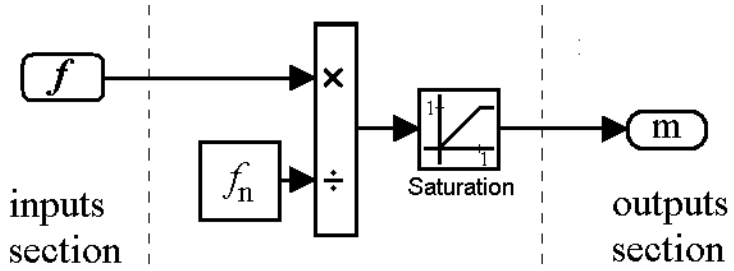

FIGURE 3: The model of *V/f* = constant controller.

Control circuits of A.C. drive system with induction motor can be divided according to different criterions. The following thinking will be focused on the fundamental properties of electric drives which are different from each other by the way of setting the required stator voltage of the motor:

1. **Variant 1:** The desired voltage may be measured and evaluated by using a suitable controller, "RI" shown in figure 4a.

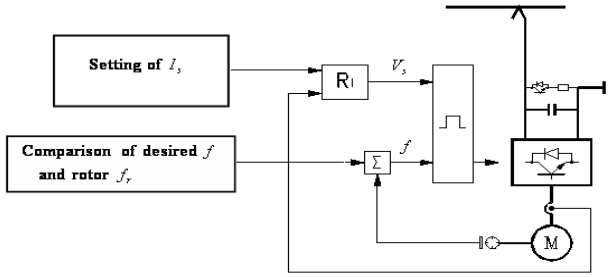

FIGURE 4A: Variant 1.

Under the effect of the variation of the load torque, the stator voltage may behave just like a disturbance that is applied to the control system. Therefore, if the current-controller, RI, is working well, then any change in the load torque will not affect the function of the motor which means that there is no need for a voltage feedback from the capacitor connected at the d.c. side of the rectifier as shown in figure 4a.

2. **Variant 2:** The stator voltage is simply estimated.

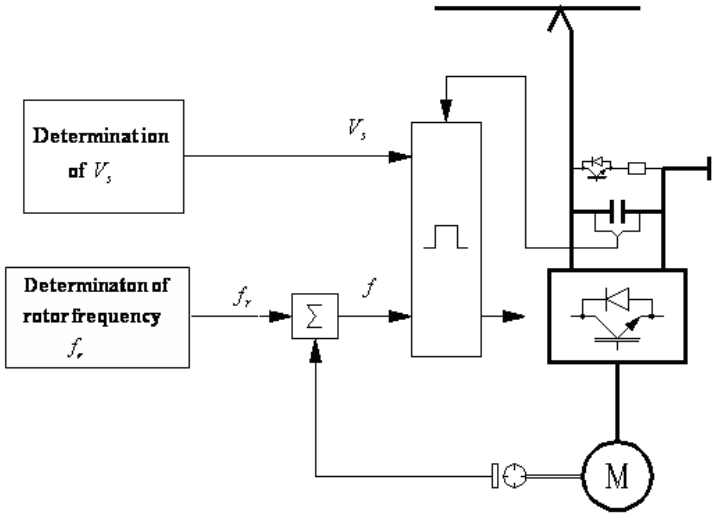

FIGURE 4B: Variant 2.

If the estimated voltage has to be equal exactly to the actual stator voltage even after it is changed, then it is necessary to take into consideration the voltage feedback from the capacitor as shown in Fig. 4b.

2.3. Modeling of Three-Phase Squirrel Cage Induction Motor

Many studies of the transient and steady state performance of induction motors have used two axes (d-q) dynamic machine model for the solution of the motor performance equations [12], while other studies have used a direct three-phase dynamic model that seemed more convenient, due to the variables involved in such modeling, in which they are the actual physical quantities of the motor [13]. Some authors have used dynamic model for small perturbations and transfer function, or solutions for dynamic behavior in complex symbolic form [14].

The steady state performances of the induction motors are obtained using static model

equations, derived from a dynamic model by setting their derivatives to zero and solving the resulting motor equations for the motor variables.

The state-space model of the squirrel cage three-phase induction motor in standard form, with respect to a synchronously rotating d-q coordinates, can be expressed as[15, 16]:

$$\left.\begin{aligned}\dot{\mathbf{x}} &= \mathbf{A}\mathbf{x} + \mathbf{B}\mathbf{u} \\ \mathbf{y} &= \mathbf{C}\mathbf{x} + \mathbf{D}\mathbf{u}\end{aligned}\right\} \quad (4)$$

Where the matrix quantities in Eq. 4 are as follows:

$\dot{\mathbf{x}} = \left[\dot{i}_{ds} \quad \dot{i}'_{dr} \quad \dot{i}_{qs} \quad \dot{i}'_{qr} \quad \dot{\omega}_m\right]^T$ -state equations vector

$\mathbf{x} = \left[i_{ds} \quad i'_{dr} \quad i_{qs} \quad i'_{qr} \quad \omega_m\right]^T$ -state vector

$\mathbf{Y} = \left[i_{ds} \quad i'_{dr} \quad i_{qs} \quad i'_{qr} \quad \omega_m \quad T_e\right]^T$ -output vector

$\mathbf{u} = \left[v_{ds} \quad 0 \quad v_{qs} \quad 0 \quad T_m\right]$-input vector

$\mathbf{D} = [0]$-direct transmission matrix

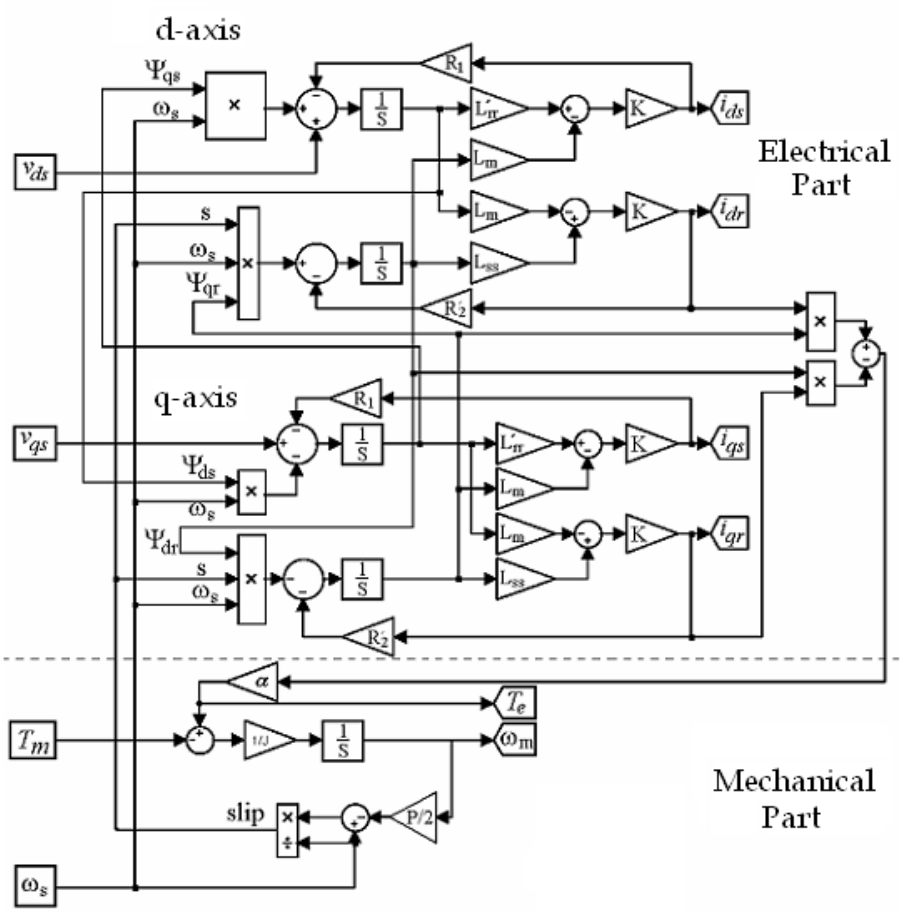

FIGURE 5: State-space model of induction motor.

$$\mathbf{A}=\begin{bmatrix} \omega_s+\frac{P}{2}\omega_m K_2 & \frac{P}{2}\omega_m K_1\frac{L_m}{L_{ss}} & \frac{R_1}{L_{ss}}K_1 & -\frac{R'_2}{L_m}K_2 & 0 \\ \frac{R_1}{L_{ss}}K_1 & -\frac{R'_2}{L_m}K_2 & -\omega_s-\frac{P}{2}\omega_m K_2 & -\frac{P}{2}\omega_m K_1\frac{L_m}{L_{ss}} & 0 \\ -\frac{P}{2}\omega_m K_1\frac{L_m}{L'_{rr}} & \omega_s-\frac{P}{2}\omega_m K_1 & -\frac{R_1}{L_m}K_2 & \frac{R'_2}{L'_{rr}}K_1 & 0 \\ -\frac{R_1}{L_m}K_2 & \frac{R'_2}{L'_{rr}}K_1 & \frac{P}{2}\omega_m K_1\frac{L_m}{L'_{rr}} & -\omega_s+\frac{P}{2}\omega_m K_1 & 0 \\ -\frac{\alpha L_m i'_{qr}}{J} & 0 & \frac{\alpha L_m i'_{dr}}{J} & 0 & 0 \end{bmatrix}$$ -state matrix

$$\mathbf{B}=\begin{bmatrix} \frac{K_1}{L_{ss}} & 0 & -\frac{K_2}{L_m} & 0 & 0 \\ 0 & \frac{K_1}{L_{ss}} & 0 & -\frac{K_2}{L_m} & 0 \\ -\frac{K_2}{L_m} & 0 & \frac{K_1}{L'_{rr}} & 0 & 0 \\ 0 & -\frac{K_2}{L_m} & 0 & \frac{K_1}{L'_{rr}} & 0 \\ 0 & 0 & 0 & 0 & -\frac{1}{J} \end{bmatrix}$$ -input matrix

$$\mathbf{C}=\begin{bmatrix} 1 & 0 & 0 & 0 & 0 \\ 0 & 1 & 0 & 0 & 0 \\ 0 & 0 & 1 & 0 & 0 \\ 0 & 0 & 0 & 1 & 0 \\ 0 & 0 & 0 & 0 & 1 \\ -\alpha L_m i'_{qr} & 0 & \alpha L_m i'_{dr} & 0 & 0 \end{bmatrix}$$ -output matrix

$\alpha=\frac{3}{4}P$ -constant; $K_1=\frac{L_{ss}L'_{rr}}{L_{ss}L'_{rr}-L^2_m}$ -constant; $K_2=\frac{L^2 m}{L_{ss}L'_{rr}-L^2_m}$ -constant

The model of mechanical part of an induction motor can be represented by:

$$T_e-T_m=J\dot{\omega}_m \tag{5}$$

Where the electromagnetic torque T_e is expressed as:

$$T_e=\frac{3}{4}PL_m(i_{qs}i'_{dr}-i_{ds}i'_{qr}) \tag{6}$$

Inputting Eq. 8 into Eq. 7, we get:

$$\dot{\omega}_m=\frac{3}{4}\frac{PL_m}{J}i_{qs}i'_{dr}-\frac{3}{4}\frac{PL_m}{J}i_{ds}i'_{qr}-\frac{1}{J}T_m \tag{7}$$

The state-space model of induction motor as electromechanical system is shown in figure 5. The parameters of simulated induction motor are given in table 1. The block diagram of the drive system studied using MATLAB Simulink is shown in figure 6.

It was noticed also that the absolute slip decreased by decreasing the frequency. The absolute slip defined as:

$$s_a = \frac{\omega_0 - \omega_m}{\omega_{0n}} \tag{8}$$

Where:

ω_0 is the no-load speed at a given frequency and ω_{0n} is the no-load at nominal frequency.

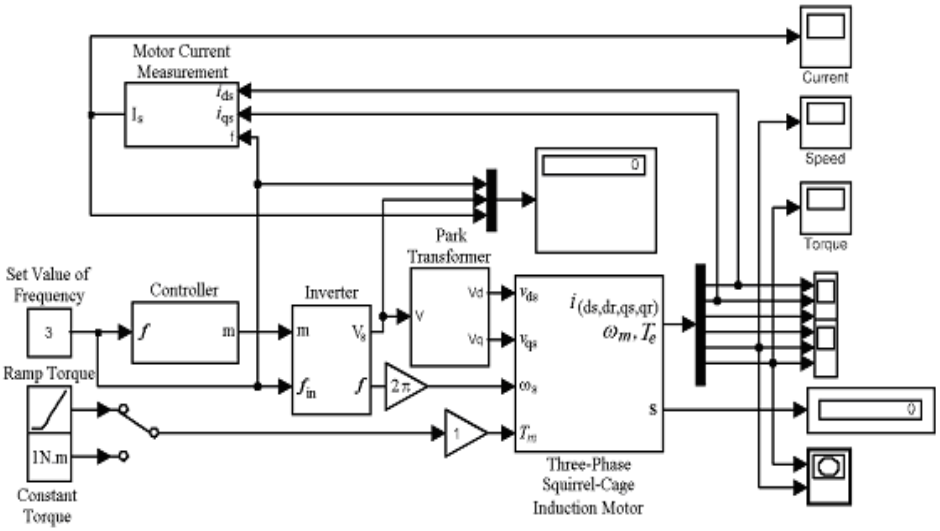

FIGURE 6: The model of the drive system.

2.4. Control With Constant Maximum Torque

The maximum torque at nominal frequency $T_{\max(n)}$ can be determined by the following equation [10]:

$$T_{\max(n)} = \frac{3PV^2 n}{8\pi f_n (R_1 + \sqrt{R^2{}_1 + X^2{}_{syn}})} \tag{9}$$

Where:

V_n = nominal value of stator voltage (phase), f_n = nominal frequency, and

$X_{syn} = X_1 + X'_2 = 2\pi f_n (L_s + L'_r)$

The maximum torque $T_{\max}$ at any frequency *f* can be determined as:

$$T_{\max} = \frac{3PV^2}{8\pi f (R_1 + \sqrt{(R^2{}_1 + (2\pi f L_s + 2\pi f L'_r)^2)})} \tag{10}$$

Equating Esq. 9 and 10, we get:

$$m = \frac{V}{V_n} = \frac{V_s}{V_n}\frac{f}{f_n}\sqrt{\frac{\frac{f_n}{f}R_1 + \sqrt{(\frac{f_n}{f})^2 R^2{}_1 + X^2{}_{syn}}}{R_1 + \sqrt{R^2{}_1 + X^2{}_{syn}}}} \tag{11}$$

Equation 11 shows that the value of the modulation index m generated for the controller with constant maximum torque is greater than that generated for the controller with $V/f = \text{constant}$. The model of $T_{\max} = \text{constant}$ controller is shown in figure 7.

The simulated mechanical characteristics of the drive system with $T_{\max} = \text{constant}$ controller are shown in figure 8, from which it is clear that the maximum torque remains constant for the

frequency range from 20Hz up to 50Hz. For frequencies below 20Hz the maximum torque has been significantly increased comparing with that of the drive system with $V/f = \text{constant}$ controller. The absolute slip has been decreased.

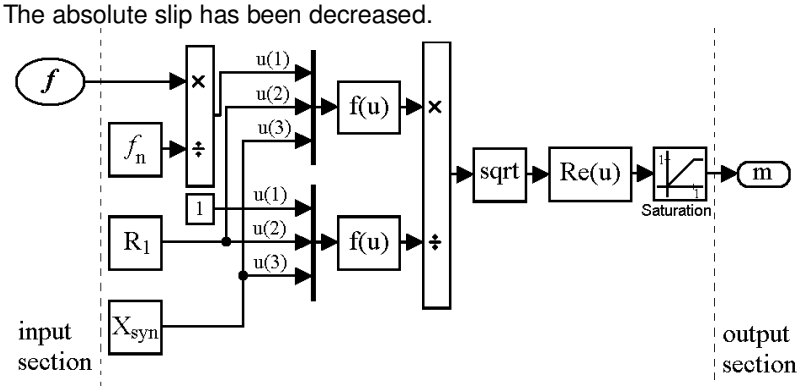

FIGURE 7: The model of $T_{\max} = \text{constant}$ controller.

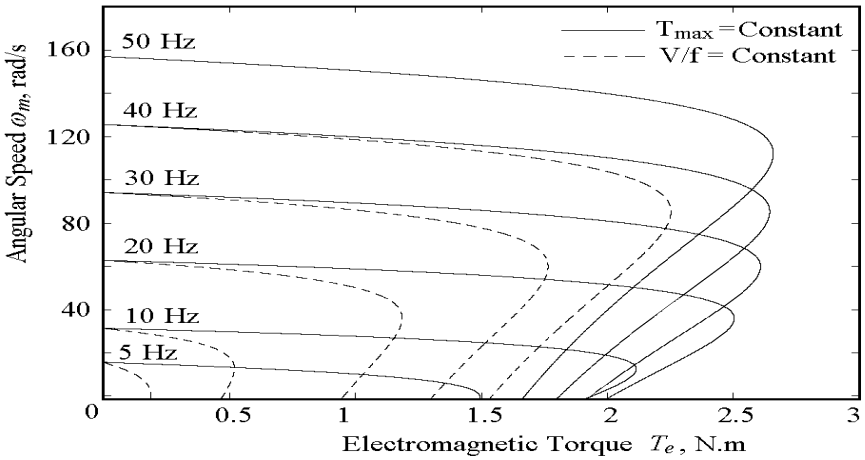

FIGURE 8: Mechanical characteristics of drive system with T_{max}= constant controller

Parameter	Value
Stator resistance R_1	65
Stator reactance X_1	40
Mutual reactance X_m	241
Rotor resistance referred to the stator R'_2	25
Rotor reactance referred to the stator X'_2	30
Nominal voltage V_n	230/400V
Nominal torque T_n	1.3N.m
Nominal input power P_n	0.25kW
Nominal current I_n	0.76A
Power factor	0.79
Nominal frequency f_n	50Hz
Number of poles P	4
Nominal speed n_n	1455 rpm
Nominal angular speed	152 rad/s
Moment of inertia J	0.02 kg.m^2

TABLE 1: Motor parameters

2.5. Control With Constant Flux

The stator flux can be kept constant, and equal to its nominal value, if the ratio of the magnetizing e.m.f. E_m to the stator frequency f remains constant, $(\frac{E_m}{f} = \frac{E_{mn}}{f_n})$. Under this condition, and based on the induction motor steady-state equivalent circuit and phasor diagram, the stator voltage V can be determined as:

$$V = K_{V/f} + R_1\sqrt{I^2{}_s - I^2{}_m} \quad (12)$$

Where:

$K_{V/f} = \frac{V}{f} = \text{constant}$, I_m = magnetizing (no-load) current.

Eq. 12 shows that the stator voltage V in the case of controller with constant flux is always greater than that of $V/f = \text{constant}$ controller. The model of controller with constant flux is shown in figure 9.

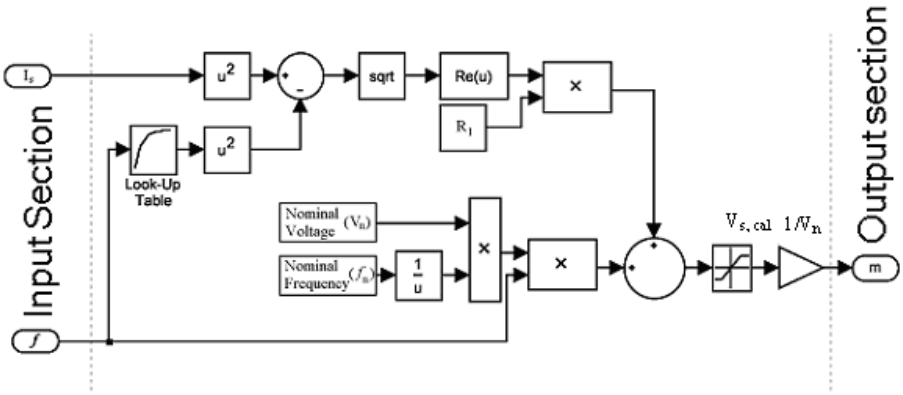

FIGURE 9: The model of ϕ = constant controller.

3. SIMULATION RESULTS

The Performance analysis of the drive system with V/f controller was provided for different values of frequency and load torque. The magnetization curve of the motor is given as follows:

$$\Psi_h = f(I_m): \begin{matrix}(I_m : \psi_h) = 0,0,29,0.24,39,0.31,60,0.38,63,0.45,80,0.5, \\ 101,0.56,132,0.63,151,0.7,\ 229,0.76,\ 311,0.83,\ 422,0.9,\ 576,0.96\end{matrix}$$

Examples of dynamic response of the system are shown in the following figures. Simulated mechanical characteristics of the drive system with different types of controllers are represented in figure 10, which shows that decreasing the frequency causes a significant increase in the maximum torque in the case of a controller with constant flux.

Figure 11 shows that the absolute slip is reduced and less than that of other types of controllers. The obtained mechanical characteristics of the drive system with constant flux controller are similar to those of drive system operating with constant power.

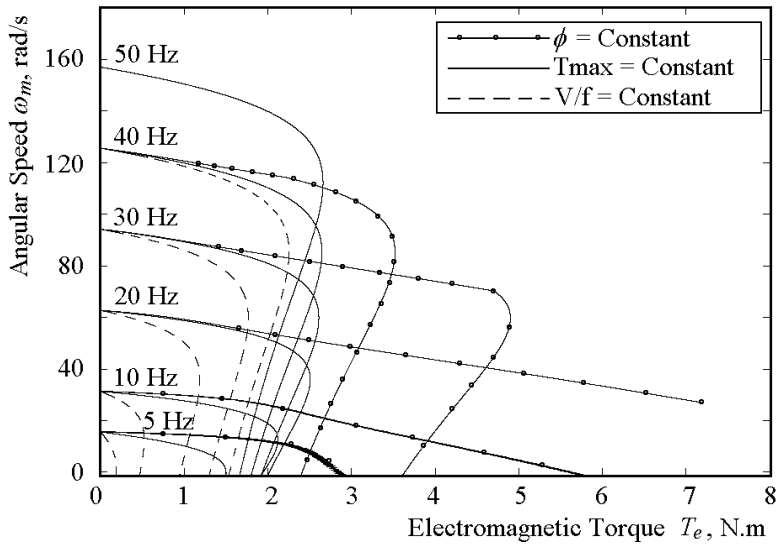

FIGURE10: Mechanical characteristics of drive system with different types of controllers.

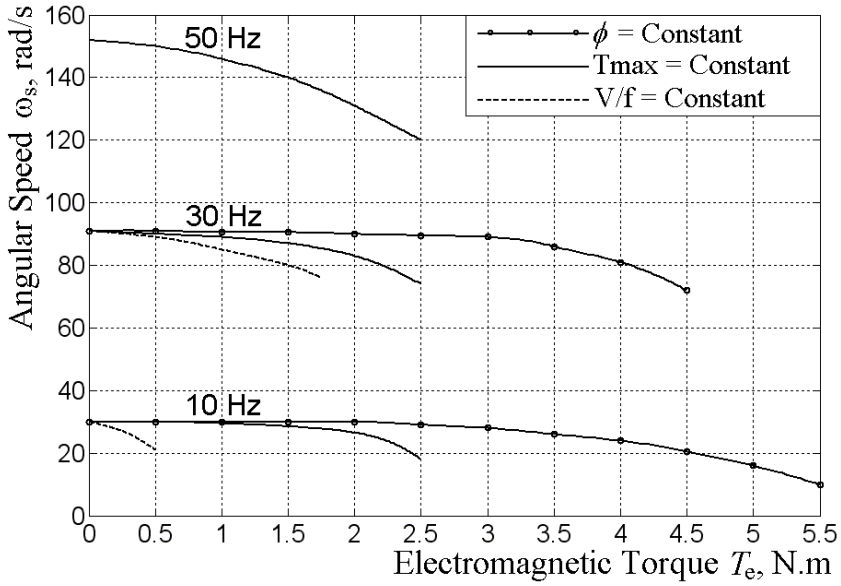

FIGURE11: Experimental mechanical characteristics of drive system with different types of controllers.

Figure (12) shows the plot of the stator voltage space vector versus the stator current space vector, $\mathbf{U_s}$ versus $\mathbf{I_s}$, the plot of the developed torque, T_e, and the *r.m.s.* value of the stator current, I_{sef} versus the rotor frequency, f_r.

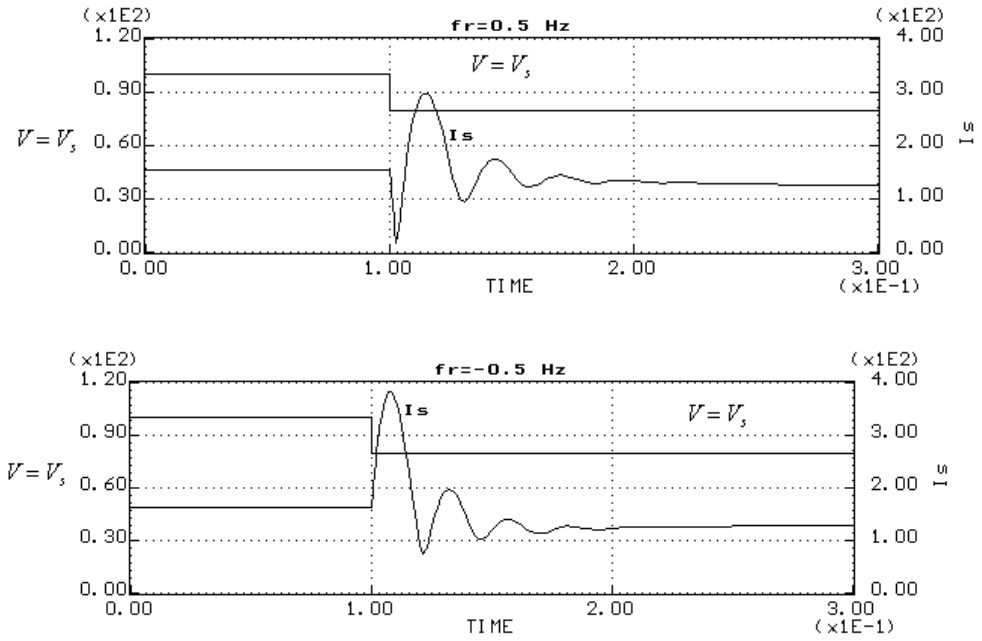

FIGURE 13: a plot of (a) V_s, I_s …abs. value of space vectors in time domain

Figure 13 shows the stator voltage and current space vectors, $\mathbf{U_s}$ and $\mathbf{I_s}$, under the condition of a variable stator voltage and constant rotor frequency. The response of the system on a change in the stator voltage while the rotor frequency is constant is adversely bad.

The results show that both the absolute value of the space vector of the stator current and the motor torque, T_e, increase with the increasing rotor frequency. The motor was not able to start at frequencies below 22Hz at load of 1.0N.m and below 11Hz at load of 0.5N.m. It was noticed also that the absolute slip, defined as $s = \frac{\omega_0 - \omega_m}{\omega_{0n}}$, is decreased with the decreasing frequency, where ω_0 is the no-load speed at a given frequency and ω_{0n} is the no-load at nominal frequency. Variation of frequency does not have significant effect on the steady-state value of stator current. Similar results were reported in [10, 11].

Therefore, if the voltage is set at the output of the controller (e.g. current), then it will cause some serious problems: during breaking regime and after reducing the voltage as it is seen in figure 13, an overshoot in the stator current is generated which is considered to be a currently known phenomenon. It could be explained by using an equivalent schematic diagram which respects the induced voltage in the stator circuit, $\frac{d\psi}{dt}$ and that in the rotor circuit, $\frac{1}{s}\frac{d\psi}{dt}$.

The simulation in figure 14 is carried out for a variable rotor frequency and constant voltage. The response to a step change in the rotor frequency is completely trouble free as it is shown in the figure. The frequency of the rotor may easily be evaluated by using a controller of any quantity, for example (e.g. Siemens, Simovert P … f_r is evaluated by using a controller of the torque component).

In order to improve the starting and load performance of the drive system under the effect of stator voltage variations, a filter is added at the output of the current controller which may have a bad effect on the dynamic properties of the current loop, especially if the loop contains further blocks with expected delay in the response. Therefore, the stator voltage V_s is set using a limiter at the output of the controller and a PI controller (K_{RI}, T_{RI}) must be added as

shown in figure 15. When the voltage decreases, the PI controller reduces the firing angle. When the voltage increases, the PI controller increases the firing angle.

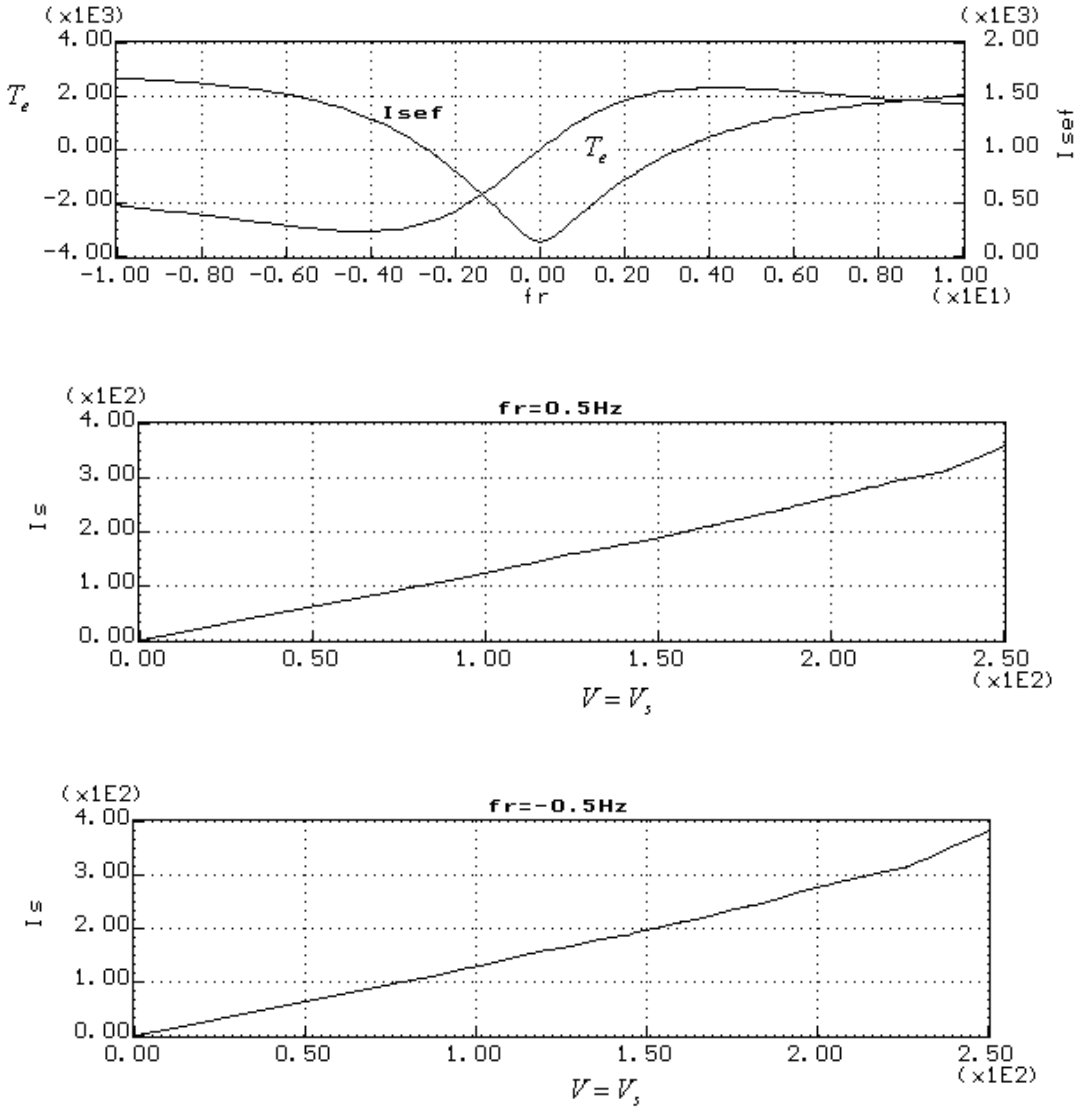

FIGURE 12: a plot of : (a) torque T_e versus rotor frequency. (b) V_s versus Is …absolute values of space vectors.

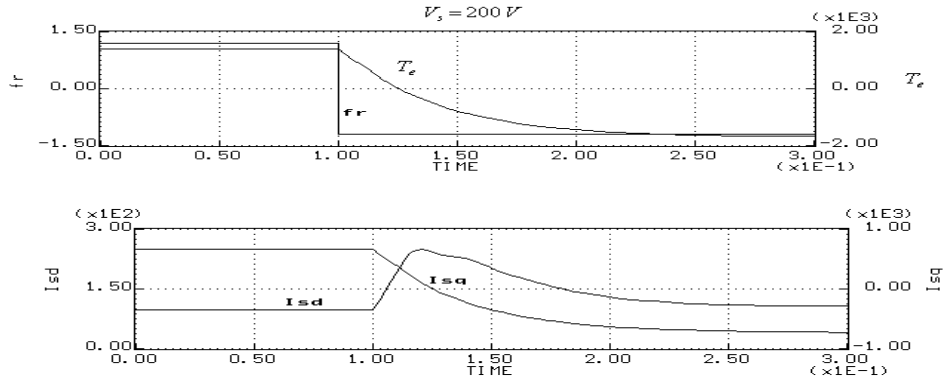

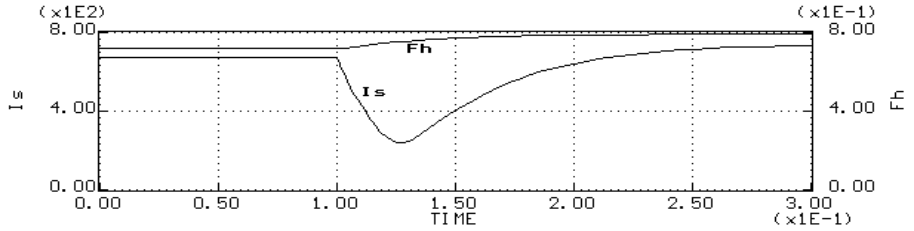

FIGURE 14: I_{sd}, I_{sq} … direct and quadrature components of stator current vector, T_e … developed torque, F_h …magnetomotive force.

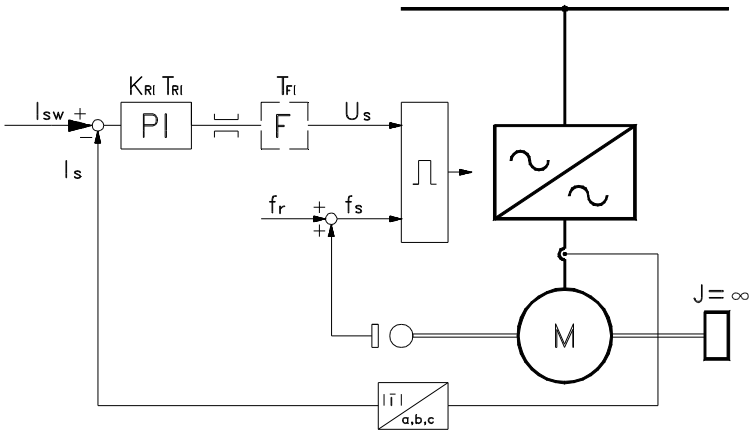

FIGURE 15: Improved control schematic topology

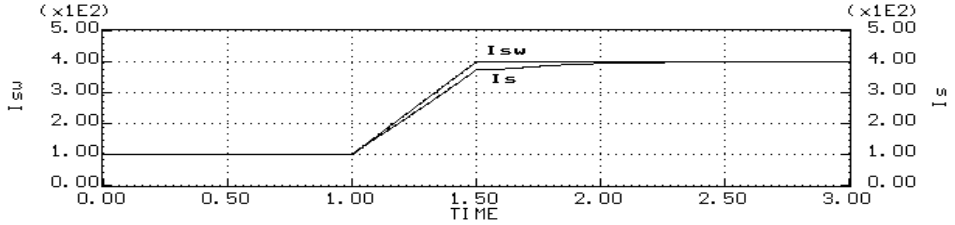

fr = 0.6 Hz, ω=2.π.40, K_{RI} = 2, T_{RI} = 0.2 s, T_{FI} = 0, I_s …absolute values of space vectors.

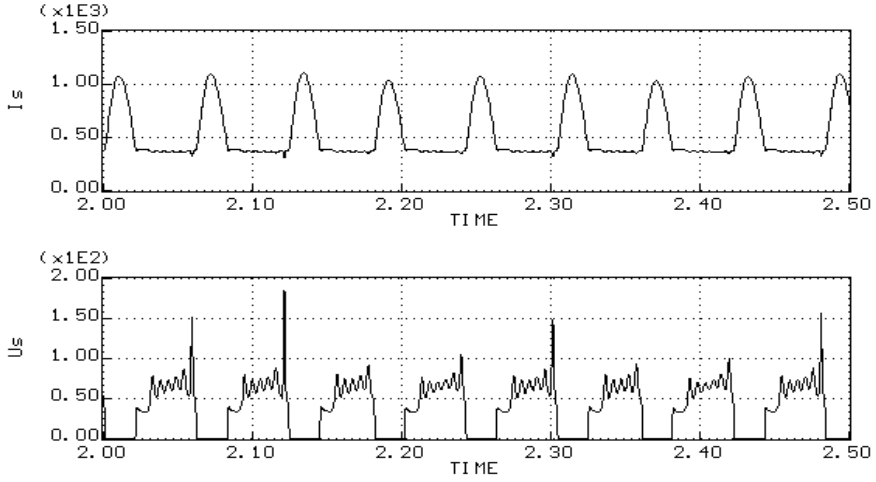

f_r = -0.6 Hz, ω=2.π.40, K_{RI} = 2, T_{RI} = 0.2 s, T_{FI} = 0.

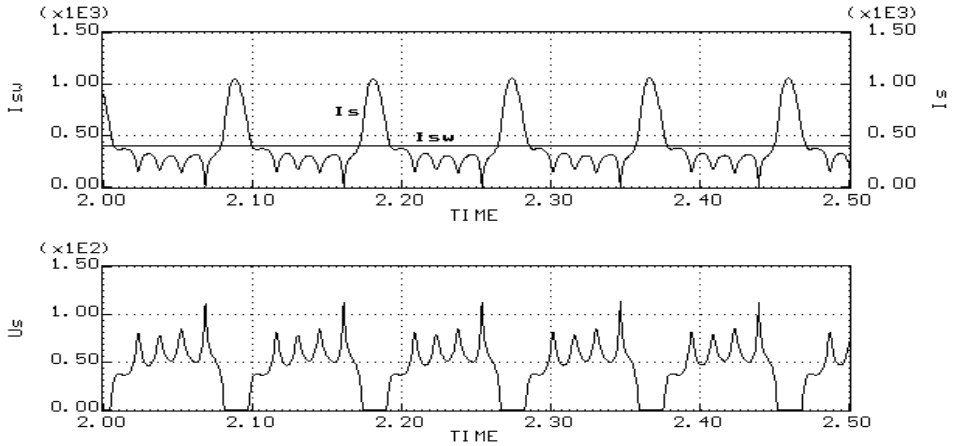

f_r = -0.6 Hz, ω=2.π.40, K_{RI} = 0.2, T_{RI} = 0.5 s, T_{FI} = 0, (small gain , without a filter).

FIGURE 16: Improved simulation results, Isw: desired r.m.s. value of I_s.

In the AC motor drive, the motor speed is not regulated in closed loop. Instead, the speed set point is used only to determine the motor voltage and frequency applied by the six-step inverter in order to maintain the (*V/f*) ratio (or the motor flux) constant from 0 to the nominal speed. Above nominal speed, the motor operates in the flux weakening mode; that is, the voltage is maintained constant at its nominal value while the frequency is increased proportionally to the speed set point. When reversing speed, a short delay is required at the zero speed crossing so that air gap flux decays to zero.

Under the above mentioned improvement conditions, figure 16 shows an improved simulation carried out for different values of rotor frequency and controller parameters.

4. CONCLUSION

Based on the results obtained in this paper, the following conclusions can be made:

1. The derived state-space model of three-phase squirrel cage induction motor can be used to analyze the performance of induction motor drive systems.
2. The implementation of constant maximum torque and constant flux controllers improves the performance of inverter-induction motor drive systems.
3. The mechanical characteristics of the drive system with constant flux controller are harder than that with constant maximum torque controller.
4. It is recommended to use constant maximum torque controller in drive systems operating with constant torque.
5. It is recommended to use constant flux controller in drive systems operating with constant power.

5. REFERENCES

[1]. R.W. De Doncker, D. W. Novonty. "The Universal Field Oriented Controller," IEEE Trans. Ind. Applicat., vol. IA-30, No 1, 1994, pp. 92-100.

[2]. R.D. Lorentz, T.A. Lipo and D.W. Novotny. "Motion Control with Induction Motors," Proceedings of IEEE, vol. 82, No. 8, 1994, pp. 1215-1240.

[3]. O.I. Okogo. "MATLAB Simulation of Induction Machine with Saturable Leakage and Magnetizing Inductances," The Pacific Journal of Science and Technology, vol. 5, No. 1, April 2003 (Spring), pp. 5-15.

[4]. A.E. Fitzgerald. " Electric Machinery," 5th Ed., McGraw-Hill, 1990.

[5]. R. Gabriel, and W. Leonhard. "Microprocessor Control of Induction Motor," IEEE/IAS Int. Sem. Power Conv. Conf. Rec., 1982, pp. 385-396.

[6]. R. Marino, S. Peresada, and P. Valigi. "Adaptive Input-Output Linearizing Control of Induction Motors," IEEE Trans. Autom. Cont., vol. 38, No. 2, 1993, pp. 208-221.

[7]. Hussein Sarhan, Rateb Al-Issa, and Qazem Jaber. "Loss-Minimization Control of Scalar Controlled Induction Motor Drives," 4th IEEE GCC Conference and Exhibition, Manama, Kingdom of Bahrain, 12th-14th Nov., 2007, p. 64.

[8]. K. Zhou and D. Wang. "Relationship Between space-Vector Modulation and Three-phase Carrier-Based PWM: A Comprehensive Analysis," IEEE Trans. Ind. Electronics, vol. 49, No. 1, 2002, pp. 186-195.

[9]. B.K. Bose. "Power Electronics and Variable Frequency Drives," IEEE Press, 1997, p. 402.

[10]. M.G. Alfredo, A.L. Thomas, and W.N. Donald. "A New Induction Motor V/f Control Method Capable of High-Performance Regulation at Low Speeds," IEEE Trans. Ind. Applicat., vol. 34, No. 4, July-august, 1998, pp. 813-820.

[11]. R. Sepe and J. Lang. "Inverter Nonlinearities and Discrete-Time Vector Current Control," IEEE Trans. Ind. Applicat., vol. 30, Jan.-Feb., 1994, pp. 62-70.

[12]. M.A. Ouhrouche. "Simulation of Direct Field-Oriented Controller for an Induction Motor Using MATLAB-Simulink Software Package," Proceedings of the IASTED International Conference Modeling and simulation, May 15-17, 2000-Pittsburgh, Penn sylvania, USA.

A Central Pattern Generator based Nonlinear Controller to Simulate Biped Locomotion with a Stable Human Gait Oscillation

Soumik Mondal *mondal.soumik@gmail.com*
Robotics & AI Lab
Indian Institute of Information Technology, Allahabad
UP-211012, India

Anup Nandy *nandy.anup@gmail.com*
LIECA - CSE/IT Department
Lovely Professional University
Punjab-144402, India

Chandrapal *cverma.ro@gmail.com*
Robotics & AI Lab
Indian Institute of Information Technology, Allahabad
UP-211012, India

Pavan Chakraborty *pavan@iiita.ac.in*
Robotics & AI Lab
Indian Institute of Information Technology, Allahabad
UP-211012, India

G. C. Nandi *gcnandi@iiita.ac.in*
Robotics & AI Lab
Indian Institute of Information Technology, Allahabad
UP-211012, India

Abstract

This paper describes the designing of a nonlinear biological controller inspired from stable human gait locomotion, which we implement for a stable biped motion on a Biped Robot. The design of a Central Pattern Generator (CPG) which consists of a four coupled Rayleigh Oscillators. A Two-Way oscillator coupling has been used for modeling the CPG. The parameters of the CPG are then optimized by Genetic Algorithm (GA) to match with the stable human gait oscillation. The stable human gait oscillation data was obtained using the Intelligent Gait Oscillation Detector (IGOD) biometric suit, which simultaneously measures both the human hips and knee oscillations. After checking the Limit Cycle behavior of the CPG it has been successfully simulated on the Spring Flamingo robot in YOBOTICS environment.

Keywords: Rayleigh Oscillator, Central Pattern Generator (CPG), Intelligent Gait Oscillation Detector (IGOD), Genetic Algorithm (GA), Nonlinear Dynamics System (NDS), YOBOTICS.

1. INTRODUCTION

Over the long decade humans have struggled to start surviving on this beautiful planet. Then the invention of rock, wheel, fire, vehicles etc. has been carried out by humans along with a tremendous innovation namely known as digital computer. Over the year's new technologies are introduced to implement human thoughts to meet certain goals in our life. Humans also proactively updated those technologies as per their own necessity. Eventually they are succeeded to develop some industrial robots which are used to perform some tasks to a limited extent. These types of robots are commonly acquainted as pre programmed robots. Then the technology took a new turn in an evolutionary approach. Gradually it has kept its own footprints in

the field of humanoid robotics with a tremendous appeal. The humanoid robots are being considered as a human being which can think rationally and act like a human to accomplish any kinds of complex task. Unlike all the activities performed by human, these humanoid robots learn to execute all the activities of human being like walking, handshaking, running etc. The humans offer maximum stress on the household robots in order to meet the completion of any kinds of household tasks. The humanoid robot can also act like a soldier in a war. The most elementary activity of humanoid robot includes walking pattern in complex environments. It offers a challenge to make the robots intelligently so that it could produce efficient walking patterns like human being in a complex environment. It includes extreme effort to deal with the complex parameters of humanoid robot for generating the accurate gait patterns in an efficient manner.

The basic concept of Central Pattern Generator (CPG) is actively related to the number of living species which produces a sequence of cyclic motor patterns. There has been represented a set of pattern generating systems or a class of neural circuits which are able to produce cyclic movements [9-11]. As per the biomechanical concept is concerned about the construction of CPG it happens to be a group constituted by the artificial neurons. These artificial neurons are called oscillators which are capable of producing an oscillatory signal output without any external periodic input. This concept of artificial neural network which is based on the central pattern generator has been used in the field of human gait biomechanics along with in robotics [11].

The main objective of this work is *"To build a CPG based model by using Rayleigh Oscillators and train this CPG by stable human gait oscillation to generate the human like biped locomotion for biped robot"*.

Contribution Done in This Paper

- ✓ Active participation of only four major joints for two legs in our work i.e. left hip, knee and Right hip, Knee.
- ✓ The design prototype of CPG model has been satisfied by establishing the coupling equation for Two-Way coupling between four different Rayleigh Oscillators for four joints to design our CPG model.
- ✓ Acquisition of the stable human walking data by a self made biometric suit called IGOD [1] and manipulates the optimized coupling parameters for our CPG model with that captured data using GA.
- ✓ Generate the human like walking pattern for the biped robot and check the stability.
- ✓ Simulate the generated human like biped locomotion by our designed CPG model into Spring Flamingo robot in YOBOTICS environment.

2. RELATED WORK

In the robotics society, we are progressively using the C.P.G. models. The different views of CPG models are designed for robots including connectionist models (e.g. Lu, Ma, Li; Arena, 2000, & Wang, 2005), and some models created by coupled oscillators (e.g. Ijspeert et al.; Kimura et al.; Williamson et al.;) [16-22]. In some infrequent cases, some spiking neural models are used (e.g. Lewis et al.) [23]. Almost all implementations consist of some sets of Coupled Differential Equations which are integrated numerically on the processor or on a microcontroller. Most likely the only exceptions that are CPGs. these CPGs are unswervingly realized in hardware, which is on a chip (e.g. Schimmel et al. 1997, DeWeerth et al.) [27] or with the analog electronics (Still & Tilden, 1998). Also up to some scope which is associated to CPG research are quasi-cyclic movements governed by chaotic maps.

The CPG models have been widely used in the control of a variety of distinct robots and also in control of different modes of locomotion. The CPG models have already been used for hexapod and octopod robots. This has been inspired by pest locomotion like Arena, Frasca, etc.

Practical implementation of CPG in knee active prosthetic limb development was proposed by G. C. Nandi et al. [12, 13]. Some CPG model simulation in Matlab was done by M. H. Kassim et al.

and A. Carlos De Filho [14, 15]. Behavior control of robot using Nonlinear Dynamics was proposed by Nakamura et al. [24-26]. Table 1 shows some more related work.

Author	Methodology	Robot
Aoi et al. [28]	Turning walk of biped robot, locomotion control using Euler angle, joint angle Lagrange equation & vision base turning control.	Biped robot
Ding et al.[29]	Motion control & dynamic modeling.	Amphibious bio-mimetic robot
Takahashi et al. [30]	Control strategy for more natural & efficient biped locomotion using Matsouka oscillator & Lagrange equation.	Mechanical model
Inada et al. [31]	CPG parameter search by genetic algorithm using Matsouka oscillator	Biped robot
Liu et al. [32]	Locomotion control using 4 mutually coupled Vanderpol oscillator.	AIBO robot
Xiao et al. [33]	Biped locomotion generation using Matsouka oscillator with parameters optimize by genetic algorithm.	Biped robot with heterogeneous leg(BRHL)
Kurita et al. [34]	Rotation, manipulation of dexterous hand using Matsouka oscillator.	Finger Gait type robot
Nishikawa et al. [35]	Dynamics of Hopf oscillator within limit cycle for designing the CPG.	Biped robot
Matsuo et al. [36]	Bio-mimetic motion control using Matsouka oscillator.	Multilink mobile robot
Osaku et al. [37]	CPG technique to swing of arm using Matsouka oscillator.	Humanoid model & environment model
Huang et al. [38]	Aim to achieve coordination to CPG & asymptotically stable walking behavior using Matsouka oscillator.	Biped robot

TABLE 1: Related Work.

3. EXPLANATION OF RELEVANT TERMS USED IN THIS PAPER

3.1 Biped Locomotion

Biped locomotion means walk or running on two legs in an upright position. Static stability on both legs is simple however maintaining a dynamic stability during locomotion is extremely difficult since it transferred from one leg to another with intermediate phase where the entire weight of the body is on one of the legs. Figure 1 describes the different phases of the biped locomotion.

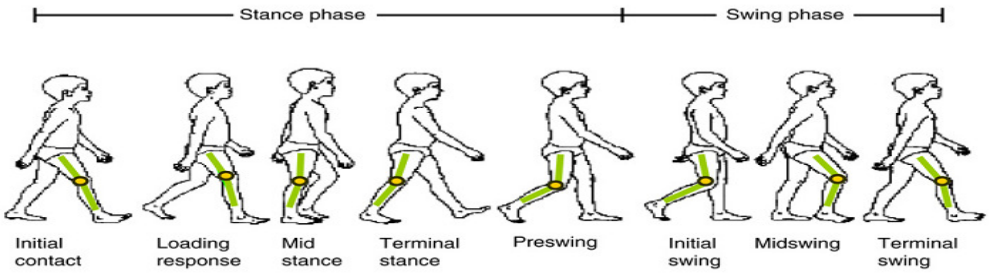

FIGURE 1: Details of biped locomotion.

3.2 Central Pattern Generator (CPG)

The concept of Central Pattern Generator is inherited from nature [3]. In this approach it is not mandatory to know the entire information about the robot dynamics. This method implies more adaptive to generate controllers for two leg walking. In this method there are some type of reflexes which are used to control the balance and the effect generated by the external force. These reflexes can also be used as the feedback for the system [2].

The CPG are oscillator based controller. So the theory of limit cycle is used and this is very well-situated for the bipedal walking phenomenon. These oscillators can regenerate the stability against some weak external input. These can persist also in the stable state on the small disturbance in the preliminary circumstances. This method can be of two types, the open loop and the closed loop method.

The concept of limit cycle was taken from Nonlinear Dynamic System *"The Limit cycle is a cycle that is isolated and closed trajectory"* [5]. Figure 2 shows the limit cycle according to the system stability.

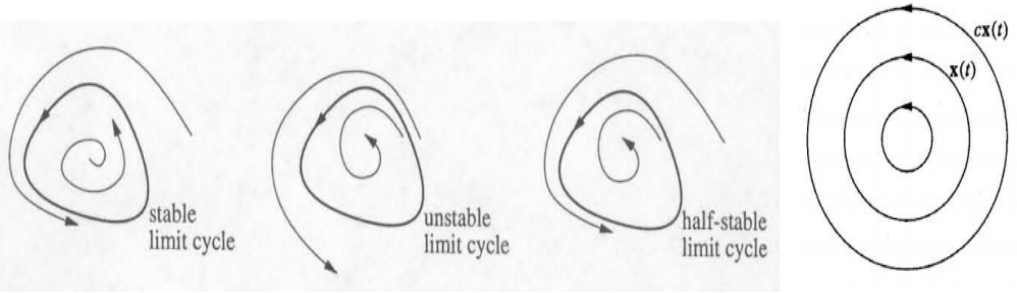

FIGURE 2: Limit Cycle according to the stability.

3.3 Intelligent Gait Oscillation Detector (IGOD)

Intelligent Gait Oscillation Detector (IGOD) is a self made rotation sensor based biometric suit which is used to capture different major joints [(Hip, Knee, Shoulder, Elbow) × 2] in terms of angle value oscillations involved in human locomotion [1]. In our work we have only considered two hip joints and two knee joints. Figure 3 depicts the rear and front view of IGOD suit. Figure 4 and 5 shows the human gait pattern for both hip joints and both knee joints respectively captured by IGOD suit for a particular person's locomotion.

FIGURE 3: (a) Rear (b) Front view of IGOD [1].

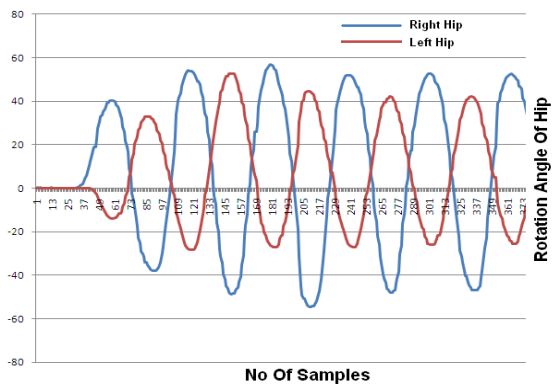

FIGURE 4: Gait pattern of both hip joints [1].

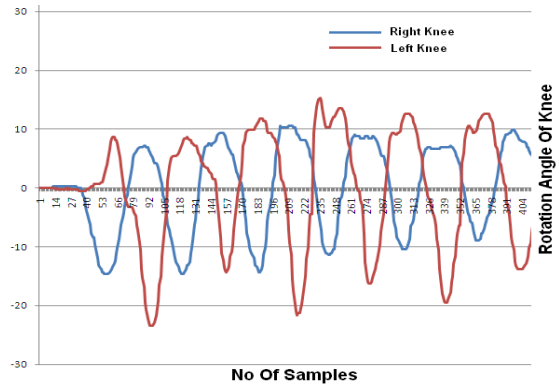

FIGURE 5: Gait pattern of both knee joints [1].

3.4 Rayleigh Oscillators

Rayleigh Oscillator is a Relaxation Oscillator. It means the oscillator is based upon performance of the physical system and with the condition of returning to the equilibrium position after being perturbed (small external force).

The second order differential equation of the Rayleigh oscillator is

$\ddot{a} - \alpha(1 - \dot{a}) + \mu^2 a = 0$ Without forced condition and

$\ddot{a} - \alpha(1 - \dot{a}) + \mu^2 a = \gamma \sin At$ For forced condition.

Here μ parameter controls the amount of voltage (energy) goes into our system. α is frequency controlling the technique in which voltage flows in the system. Now we are trying to show that how different parameters of this oscillator will affects the pattern. Figure 6 represents the Matlab plot of **a** vs. time **t** and Figure 7 represents the limit cycle of a Rayleigh Oscillator where α=1, μ=0.5, p=1. Figure 8 show that **a** vs. **t** plot where α=1, μ=0.5, p=50 and Figure 9 show that **a** vs. **t** plot where α=1, μ=0.2, p=1.

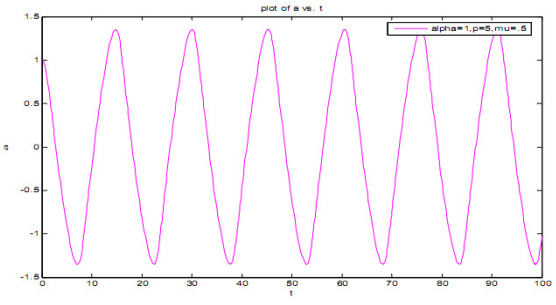

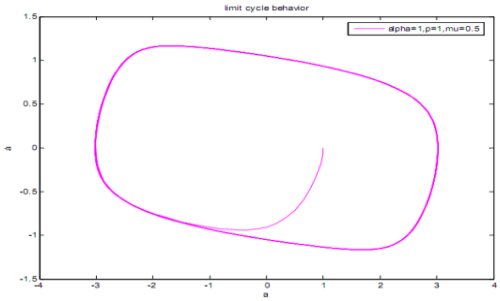

FIGURE 6: Plot of **a** vs. time **t.** where α=1, μ=0.5. **FIGURE 7:** Limit Cycle of Rayleigh Oscillator where α=1, μ=0.5, p=1.

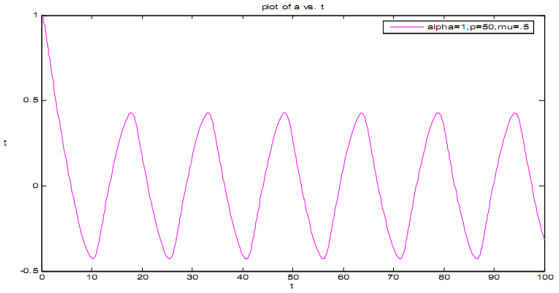

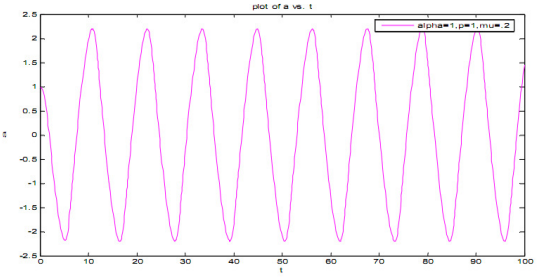

FIGURE 8: Plot of **a** vs. time **t.** where α=1, μ=0.5, p=50.

FIGURE 9: Pot of **a** vs. time **t.** where α=1, μ=0.2, p=1.

3.5 YOBOTICS SIMULATOR

YOBOTICS is a simulation tool for robot simulation. It is a very good software package to simple and rapidly generating simulations for mechanical system like biped locomotion, biomechanical model regarding robots [4]. This simulator has Java based API. Figure 10 shows the different components of YOBOTICS robotics simulation tool.

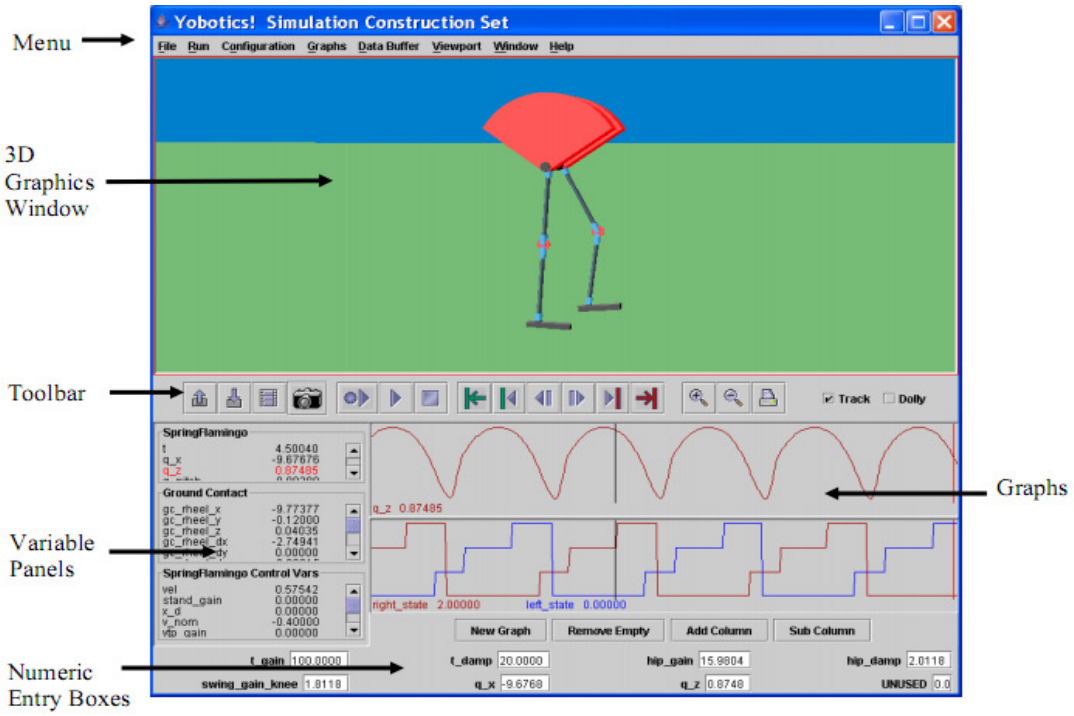

FIGURE 10: GUI window of YOBOTICS simulation software with a Spring Flamingo robot.

4. MODELING THE CPG

In our work we modeled the CPG according to the concept of Nonlinear Dynamic System (NDS). According to the NDS concept if we can couple the relaxation oscillators then the system can be able to produce different rhythmic patterns and also we can be able to check the system stability according to this concept. The CPG model with all four Two-Way coupled Rayleigh oscillators is shown in Figure 11 (a) and Figure 11 (b) showing the different coupling parameters.

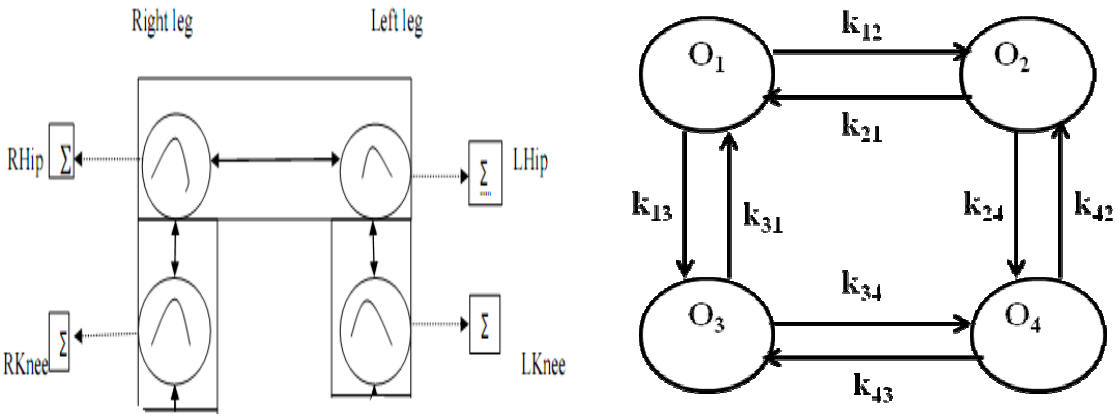

FIGURE 11: CPG Model (a) Oscillators position with Two-Way coupling and (b) Different coupling parameters.

In this figure O_1, O_2, O_3, O_4 represent four Rayleigh oscillators. k_{12}, k_{21} are coupling parameters between oscillator O_1 and O_2. k_{24}, k_{42} are parameters between oscillator O_1 and O_4. The parameters between oscillator O_3 and O_4 are k_{34} and k_{43}, and k_{31}, k_{13} are parameter between oscillator O_1 and O_3.

4.1 Rayleigh Oscillator Coupling

As we already did the basic architecture of the modeling of the CPG then the implementation phase comes into under consideration. The implementations are categorized into two different parts.

First part in our model, we started placing the Rayleigh oscillators at the different rhythm generating position i.e. left side knee, right side knee, left side hip and right side hip location. These four Rayleigh oscillators are as follows that are in the form of second order differential equation.

For Right side Hip oscillator equation: $\ddot{a}_1 - \alpha_1 (1-d_1 \acute{a}_1^2) \acute{a}_1 + \mu_1^2 (a_1-a_{10}) = 0$ -------- (A)
For the Left side Hip oscillator equation: $\ddot{a}_2 - \alpha_2 (1-d_2 \acute{a}_2^2) \acute{a}_2 + \mu_2^2 (a_2-a_{20}) = 0$ --------- (B)
For the Right side Knee oscillator equation: $\ddot{a}_3 - \alpha_3 (1-d_3 \acute{a}_3^2) \acute{a}_3 + \mu_3^2 (a_3 - a_{30}) = 0$ -------- (C)
For Left side Knee oscillator equation: $\ddot{a}_4 - \alpha_4 (1-d_4 \acute{a}_4^2) \acute{a}_4 + \mu_4 (a_4 - a_{40}) = 0$ ---------- (D)

Here these parameter d_1, d_2, d_3, d_4, μ_1^2, μ_2^2 μ_3^2 μ_4^2, α_1, α_2, α_3, α_4 refer to positive constants in the Rayleigh oscillators. Changing these parameters permit the modification of the frequency of generated signal and amplitude of generated signal.

Solve the second order differential equation is very complicated. So, now we are representing the first order equation of A, B, C and D are written below:

Form equation (A) we found
$\acute{a}_1 = z_1$ and $\acute{z}_1 = \alpha_1 (1-d_1 z_1^2) z_1 - \mu_1^2 (a_1 - a_{10})$ ---------- (e)
Form equation (B) we found
$\acute{a}_2 = z_2$ and $\acute{z}_2 = \alpha_2 (1-d_2 z_2^2) z_2 - \mu_2^2 (a_2 - a_{20})$ ---------- (f)
Form equation (C) we found
$\acute{a}_3 = z_3$ and $\acute{z}_3 = \alpha_3 (1-d_3 z_3^2) z_3 - \mu_3^2 (a_3 - a_{30})$ ---------- (g)
Form equation (D) we found
$\acute{a}_4 = z_4$ and $\acute{z}_4 = \alpha_4 (1-d_4 z_4^2) z_4 - \mu_4^2 (a_4 - a_{40})$ --------- (h)

The four Rayleigh oscillators in our model will produce four output signals autonomously. Here, all oscillators are not affecting each other because there is no coupling. In order to produce the preferred rhythmical output pattern next task is to be linked with all oscillators with each other or coupling them.

Secondly we have done interconnection among all the four oscillators related with each other. In this work the coupling concept has been introduced which basically includes two types of coupling. One is refereeing One-Way coupling and other is directing to Two-Way coupling. In this paper a Two-Way coupling technique has been applied. In Two-Way coupling type, if two or more oscillators are interrelated then all the oscillators' effect on each other. It has been observed that first oscillator effects on second oscillator and second oscillator effects on first one for linking the all of four Rayleigh oscillators that are used for left side knee, right side knee, left side hip and right side hip location. In order to provide encouragement this idea came from the association among left side knee, right side knee, left side hip and right side hip joints of humans at the time of simple walking. If we talk about biped locomotion in human being a situation is arrived at locate one leg is in stance phase (on ground) the other side leg is in the situation of swing phase (in air) [refer to Fig. 1]. As a result, we can always exempt phase association stuck between the left side knee's joint angle & right side knee's joint angle the hip angle differently other is knee joint angles are synchronized. If we talk about hip difference angle then we can say that it gives an oscillatory performance throughout locomotion, angle difference oscillates in mean while positive value and

then negative values.

Therefore all the four oscillators are interlinked to do so facts discussed in above section. These second order differential equation showing all four oscillators has considered only one term in account of feedback from one to other oscillator. Following are the equation for this system after coupling oscillators:

$$\ddot{a}_1 - \alpha_1 (1 - d_1 \acute{a}_1^2) \acute{a}_1 + \mu_1^2 (a_1 - a_{10}) - k_{13} (\acute{a}_3 (a_3 - a_{30})) - k_{12} (\acute{a}_1 - \acute{a}_2) = 0 \text{ ---- (i)}$$

$$\ddot{a}_2 - \alpha_2 (1 - d_2 \acute{a}_2^2) \acute{a}_2 + \mu_2^2 (a_2 - a_{20}) - k_{24} (\acute{a}_4 (a_4 - a_{40})) - k_{21} (\acute{a}_2 - \acute{a}_2) = 0 \text{ ---- (j)}$$

$$\ddot{a}_3 - \alpha_3 (1 - d_3 \acute{a}_3^2) \acute{a}_3 + \mu_3^2 (a_3 - a_{30}) - k_{31} (\acute{a}_1 (a_1 - a_{10})) - k_{34} (\acute{a}_3 - \acute{a}_4) = 0 \text{ ---- (k)}$$

$$\ddot{a}_4 - \alpha_4 (1 - d_4 \acute{a}_4^2) \acute{a}_4 + \mu_4^2 (a_4 - a_{40}) - k_{42} (\acute{a}_2 (a_2 - a_{20})) - k_{43} (\acute{a}_4 - \acute{a}_3) = 0 \text{ ---- (l)}$$

4.2 Optimization of CPG Parameters Using GA

Now we need to optimize the different parameters of CPG. In our work we choose Genetic Algorithm (GA) as an optimization technique. The fitness function for GA is the difference between angles that is joint angles generated by our CPG model and the joint angle captured by IGOD suit. Here e(t) is the difference between the angle value in time **t**. So the fitness function is

$$E_d(t) = \beta_1 e(t) + \beta_2 de(t) / dt + \beta_3 \int e(t)\, dt \text{ ------- (p)}$$

β_1, β_2 and β_3 considered as Proportional Constant, Differential Constant and Integral Constant respectively. According to our fitness function reduce the function value means reduce the angle difference that means we are going towards the generation of natural human like walking pattern by our CPG model for our robot.

Now differentiating the equation (p) with respect to t :

$$\beta_1 \, de(t)/dt + \beta_2 \, d^2e(t)/dt^2 + \beta_3 \, e(t) = dE_d(t)/dt \text{ -- (q)}$$

Now consider that the system is in steady state condition that means system within the virtual static state. In condition of steady state is $de(t)/dt \rightarrow 0$, $d^2e(t)/dt^2 \rightarrow 0$. We know that $E_d(t)$ is constant and $\beta_3 e(t) = 0$, but β_3 is not equals to 0 because this is considered as positive constant, that means $e(t) \rightarrow 0$ **------- (r).**

Hence we can say that the fitness function reduces the fault. Therefore the fitness function (p) will decrease the steady state error to 0.

5. ANALYSIS OF OUR CPG MODEL

In this part we will show the CPG parameters we obtain from GA and the walking pattern generated by our CPG model. In our work the fitness function (p) is converged to 0.001, that means $e(t) \rightarrow 0.001$. So the optimized value we get from GA is k_{12}=.2111, k_{13}=.1125, k_{24}=.1129, k_{21}=.3010, k_{31}=.1125, k_{34}=.2012, k_{42}=.1129, k_{43}=.2012, α_1=.0314, α_2=.0220, α_3=.0208 and α_4=.0308.

Figure 12 shows the rhythmic patterns generated by our CPG model.

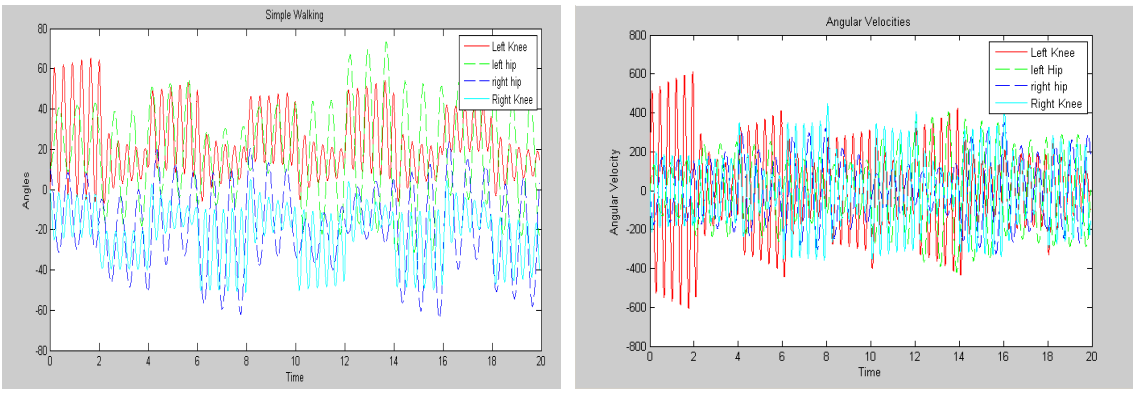

FIGURE 12: The pattern generated by our CPG model of different joints (a) Angle vs. Time graph were angle is in degree and time is in Second. (b) Velocity vs. Time graph.

Now coming to the phase space trajectory graphs those are also known as limit cycle which should be in stable state for stable walking of a Robot. Figure 13, 14, 15 and 16 shows the phase space trajectory graph for left knee, left hip, right knee and right hip respectively. All these phase diagram start from Origin and converged to constant oscillatory swinging action and have a stable limit cycle.

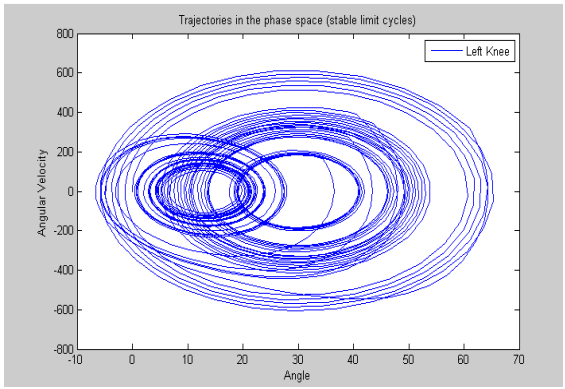

FIGURE 13: Phase diagram of Left Knee joint.

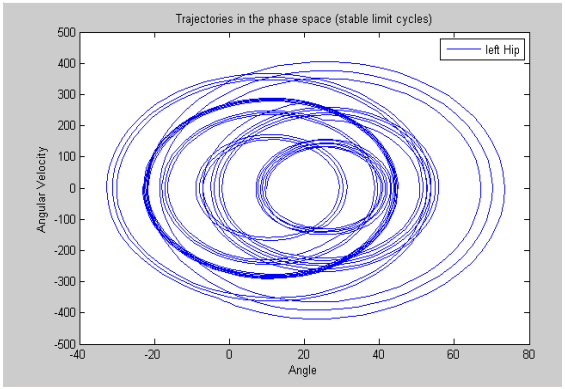

FIGURE 14: Phase diagram of Left Hip joint.

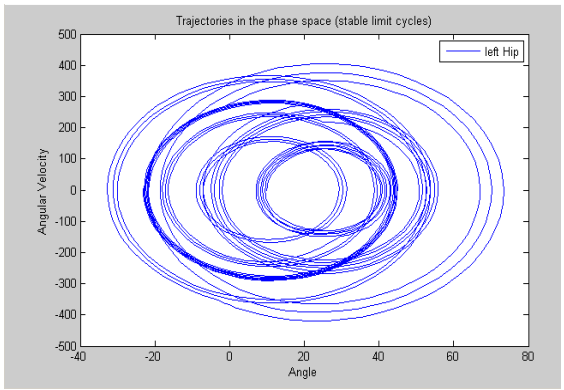

FIGURE 15: Phase diagram of Right Knee joint.

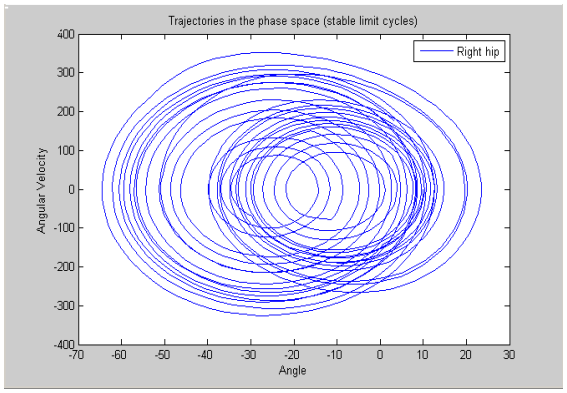

FIGURE 16: Phase diagram of Right Hip joint.

6. SIMULATION

In our work we have used Matlab 7.5 and YOBOTICS robotics simulation environment. The Differential equation solver presented in Matlab 7.5 is used for modeling the CPG. The

implementation part of GA is also done in Matlab 7.5. This experiment provides us some patterns those are being tested on YOBOTICS simulator with a Spring Flamingo Robot. It also gives the oscillatory activity of the CPG where angle are considered in radian.

In this environment spring damper system is used for modeling the ground. The coefficient of the spring is 40000N/m and 100N/m for damping. The Ts is time interval having value 0.5ms. The pattern we have got from CPG given to this simulator is in the form of CSV (Comma Separated Value) file format. In this simulator we can export the CSV file and run it freely. Since CPG is matched to an actual human gait oscillation; the ratio of the limb dimension has been kept similar to that of a human. After running it we will get the pattern and intended to prove of our CPG model is working or not. Figure 17 is the snap shot of a walking Spring Flamingo robot from three camera view in YOBOTICS environment. Figure 18 shows the each joint oscillation activity when the Spring Flamingo robot is walking. Figure 19 shows the state diagram of our robot within a particular gait cycle when the robot is walking. Figure 20 shows the plot of the robot state diagram.

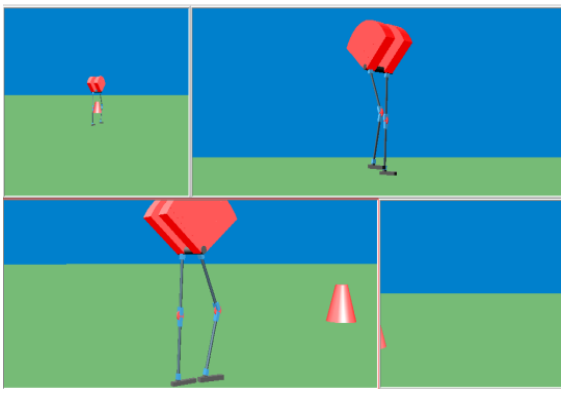

FIGURE 17: Walking of a Spring Flamingo robot.

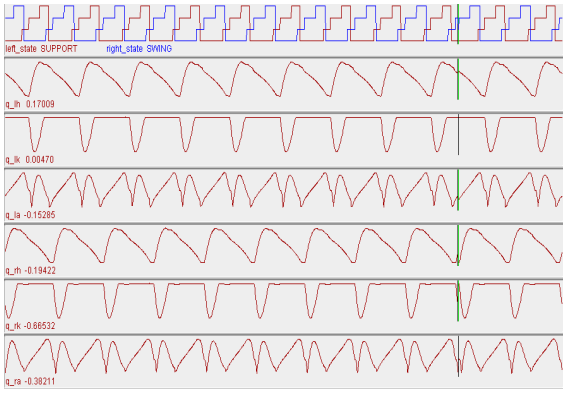

FIGURE 18: Oscillation activity of each joint.

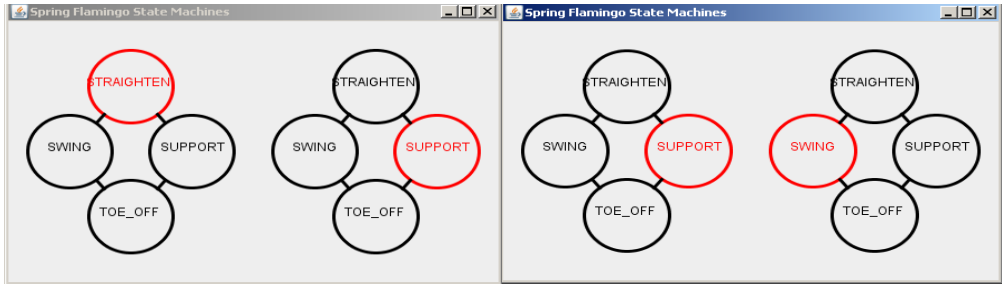

FIGURE 19: Shows the state of left and right legs when the robot is walking. (A) Left leg is in straightening state while right is in support state. (B) Left leg is in support state while right is in swing state.

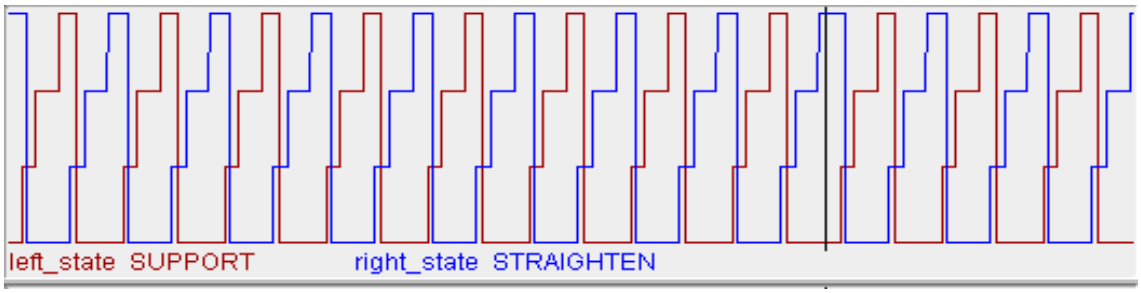

FIGURE 20: Plot of the state diagram when the robot is walking.

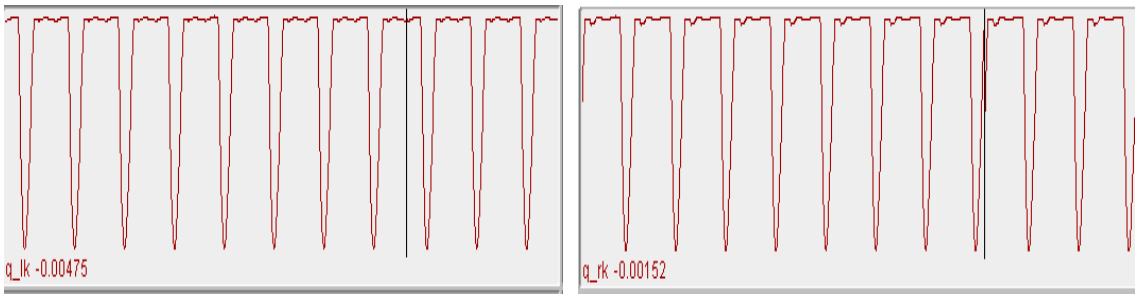

FIGURE 21: Angle (in radian) vs. Time (in ms) graph (a) for left knee and (b) for right knee.

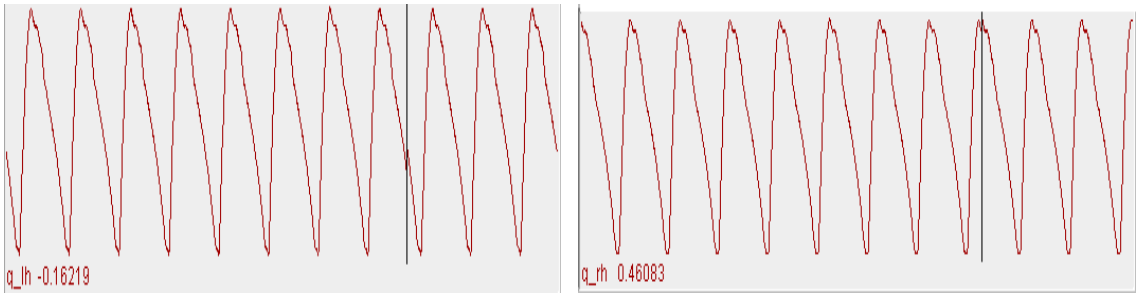

FIGURE 22: Angle (in radian) vs. Time (in ms) graph (a) for left hip and (b) for right hip.

Figure 21 (a), 21 (b), 22 (a), 22 (b) shows the different robot joint oscillations (e.g. left knee, right knee, left hip and right hip respectively) angle (in radian) vs. time (in ms) plot. All these four figures are extremely correlated with the actual human data captured by the IGOD suit [refer to Figure 4 and 5].

7. CONSLUSION & FUTURE WORK

In our entire research work we have shown the major contribution of Rayleigh oscillator for the modeling of the nonlinear based CPG controller for biped locomotion. This model involves only four joints in our research work. It allows us to measure the accurate gait pattern influenced by four joints. The application of CPG based model can be depicted on humanoid robot HOAP 2 (Humanoid Open Architecture Platform 2) to deal with 26 joints of full body oscillation. An exclusive CPG based controller can be designed to generate accurate gait pattern for biped oscillation of humanoid robot. A Sensory feedback control can be considered to deal with perturbation like wind slopes etc to give huge impact on nonlinear dynamical system. The sensory feedback control is pertaining with the extension of sensory inputs which are needed to deal with the environment in an interactive way.

It is a very complex task to generate rhythmic movement of bipedal robot. So a CPG based model has been constructed using Rayleigh oscillator inspired by biologically CPG based model. It gives us drawbacks which can be resolved by another technique called CPG based controller using MATSUOKA oscillator [6-8]. In this work we have considered only 4 major joints to simulate the gait oscillations but the inclusion of more other joints of human body indicates the construction of a robust nonlinear oscillator for generation of rhythmic pattern of bipedal robot. Despite of the simulation work presented on human gait oscillation we would suggest to use this nonlinear controller on real humanoid robot in the real environment.

Acknowledgments
This work was supported by Indian Institute of Information Technology, Allahabad, India. The preliminary work is going to publish in the proceedings of 4th Int. Conf. on Contemporary Computing, 2011.

8. REFERENCES

[1] S. Mondal, A. Nandy, A. Chakrabarti, P. Chakraborty and G. C. Nandi. "A Framework for Synthesis of Human Gait Oscillation Using Intelligent Gait Oscillation Detector (IGOD)". In Proceedings of the 3rd International Conference on Contemporary Computing, Springer-Verlag CCIS, vol. 94, Contemporary Computing, Part 7, pp. 340-349, 2010.

[2] G. Taga. "A model of the neuro- musculo-skeletal system for anticipatory adjustment of human locomotion during obstacle avoidance". Biological Cybernetics,78(1): 9-17, 1998.

[3] W. QiDi, L. ChengJu, Z. JiaQi and C. QiJun. "Survey of locomotion control of legged robot inspired by biological concept". Information Science, Springer, Science in China Series F, pp. 1715-1729, 2009.

[4] Website of the dynamics simulation software YOBOTICS [online], http//yobitics.com/simulation/simulation.htm.

[5] A. Pikovsky, M. Rosenblum and J. Kurths. "Synchronization, A universal Concept in non-linear sciences". Cambridge University Press, 2001.

[6] K. Matsuoka. "Sustained oscillations generated by mutually inhibiting neurons with adaptation". Biological Cybernetics, 52: 367-376, 1985.

[7] K. Matsuoka. "Mechanisms of frequency and pattern control in the neural rhythm generators". Biological Cybernetics, 56: 345-353, 1987.

[8] M. M. Williamson. "Design Rhythmic Motions using Neural Oscillators". In Proceedings of the IEEE/RSJ IROS'99, 1999.

[9] S. Grillner. "Control of locomotion in bipeds, tetrapods and fish". Brooks V B (ed). Handbook of Physiology, Sect. I: The Nervous System II, Motor Control. American Physio- logical Society, Waverly Press, Bethesda, Maryland, 1981.

[10] A. H. Cohen, S. Rossignol and S. Grillner. "Neural Control of Rhythmic Movements in Vertebrates". John Wiley & Sons, New York, 1998.

[11] J. J. Abbas and R. J. Full. "Neuromechanical interaction in cyclic movements". Winters J M, Crago P E (eds). Biome- chanics and Neural Control of Posture and Movement. Spring-Verlag, New York, 2000.

[12] G. C. Nandi, A. J. Ijspeert and A. Nandi. "Biologically inspired CPG based above knee active prosthesis". In Proceedings of the IEEE/ RSJ IROS'08, 2008.

[13] G. C. Nandi, A. J. Ijspeert, P. Chakraborty and A. Nandi. "Development of Adaptive Modular Active Leg (AMAL) using bipedal robotics technology". Robotics and Autonomous Systems, 57: 603-616, 2009.

[14] M. H. Kassim, N. Zainal and M. R. Arshad. "Central Pattern Generator in Bio-inspired Simulation using MATLAB". In Proceedings of the MEDINFO'98, 1998.

[15] A. C. De P. Filho. "Simulating the Hip and Knee Behavior of a Biped by Means of Nonlinear Oscillators". Open Cybernetics and Systemics Journal, 2: 185-191, 2008.

[16] A. J. Ijspeert. “Central Pattern Generators for locomotion control in animals and robots: A review”. Neural Networks, 21: 642-653, 2008.

[17] A. J. Ijspeert, A. Crespi, D. Ryczko and J. M. Cabelguentics. “From swimming to walking with a salamander robot driven by a spinal cord model”. Science, 315: 1416-1420, March 2007.

[18] A. J. Ijspeert, A. Crespi and J. M. Cabelguentics. “Simulation and robotics studies of salamander locomotion: Applying neurobiological principles to the control of locomotion in robotics”. Neuroinformatics, 3: 171-195, 2005.

[19] H. Kimura, Y. Fukuoka and A. H. Cohen. “Adaptive dynamic walking of a quadruped robot on natural ground based on biological concepts”. International Journal of Robotics Research, 26: 475-490, 2007.

[20] H. Kimura, A. Akiyama and K. Sakurama. “Realization of dynamic walking and running of the quadruped using neural oscillators”. Autonomous Robots, 7: 247-258, 1999.

[21] H. Kimura, K. Tsuchiya, A. Ishiguro and H. White. “Adaptive Motion of Animals and Machines”. Springer-Verlag, 2005.

[22] M. M. Williamson. “Robot arm control exploiting neural dynamics”. PhD Thesis, MIT, Cambridge, MA, June 1999.

[23] M. A. Lewis, F. Tenore and R. E. Cummings. “CPG design using inhibitory neurons”. In Proceedings of the IEEE/ RSJ ICRA’05, 2005.

[24] A. Sekiguchi and Y. Nakamura. “Behavior Control of Robot Using Orbits of Nonlinear Dynamics”. In Proceedings of the IEEE/RSJ ICRA’01, 2001.

[25] Y. Nakamura, T. Yamazaki and N. Mixushima. “Synthesis, Learning and Abstraction of Skills through Parameterized Smooth Map from Sensors to Behaviors”. In Proceedings of the IEEE/RSJ ICRA’99, 1999.

[26] A. Sekiguchi and Y. Nakaniura. “The Chaotic Mobile Robot”. In Proceedings of the IEEE/RSJ International Conference on Intelligent Robots and Systems, 1999.

[27] C. A. Williams and S. P. DeWeerth. “Resonance tuning of a neuromechanical system with two negative sensory feedback configurations”. Neurocomputing, 70(10-12): 1954-1959, June 2007.

[28] S. Aoi, K. Tsuchiya and K. Tsujita. “Turning control of a biped locomotion robot using nonlinear oscillators’’. In Proceedings of the IEEE/RSJ ICRA’04, 2004.

[29] R. Ding, J. Yu, Q. Yang, M. Tan and J. Zhang. “CPG based dynamics modeling and simulation for a bio-mimetic amphibious robot”. In Proceedings of the IEEE International Conference on Robotics and Bio-mimetic, 2009.

[30] M. Takahashi, T. Narukawa, K. Miyakawa and K. Yoshida. “Combined control of CPG and torso attitude control for biped locomotion”. In Proceedings of the IEEE/RSJ IROS’05, 2005.

[31] H. Inada and K. Ishii. “Behavior generation of biped robot using Central Pattern Generator (CPG), (1st report: CPG parameter searching method by genetic algorithm)”. In Proceedings of the IEEE/RSJ IROS’03, 2003.

[32] C. Liu, Q. Chen and J. Zhang. “Coupled Van Der Pol oscillators utilised as central pattern generators for quadruped locomotion”. In Proceedings of the 21st annual international conference on Chinese control and decision conference, 2009.

[33] J. Xiao, J. Su, Y. Cheng, F. Wang and X. Xu. “Research on gait planning of artificial leg based on central pattern generator”. In Proceedings of the Control and Decision Conference, 2008.

[34] Y. Kurita, J. Ueda, Y. Matsumoto and T. Ogasawara. “CPG-based manipulation: generation of rhythmic finger gait from human observation”. In Proceedings of the IEEE/RSJ ICRA’04, 2004.

[35] I. Nishikawa, K. Hayashi and K. Sakakibara. “Complex-valued neuron to describe the dynamics after hopf bifurcation: an example of CPG model for a biped locomotion”. In Proceedings of the International Joint Conference on Neural Network, 2007.

[36] T. Matsuo, T. Yokoyama and K. Ishii. “Bio-mimetic motion control system using CPG for a multi link mobile robot”. In Proceedings of the Annual Conference, The University Electro-Communications, japan, 2008.

[37] K. Osaku, H. Minakata and S. Tadakuma. "A study of CPG based walking utilizing swing of arms". In Proceedings of the 9th IEEE International Workshop on Advanced Motion Control, 2006.

[38] W. Huang, C. M. Chew and G. S. Hong. "Coordination in CPG and its Application on Bipedal Walking". In Proceedings of the IEEE Conference on Robotics, Automation and Mechatronics, 2008.

Semi-Autonomous Control of A Multi-Agent Robotic System for Multi-Target Operations

Yushing Cheung *ycheung@stevens.edu*
Department of Mechanical Engineering,
Stevens Institute of Technology,
Hoboken, NJ 07030, USA

Jae H. Chung *jchung3@stevens.edu*
US Army RDECOM-ARDEC,
Building 95N,
Picatinny Arsenal, NJ 07806, USA

Abstract

Since multi-targets often occur in most applications, it is required that multi-robots are grouped to work on multi-targets simultaneously. Therefore, this paper proposes a control method for a single-master multi-slave (SMMS) teleoperator to control cooperative mobile multi-robots for a multi-target mission. The major components of the proposed control method are the robot-target pairing method and modified potential field based leader-follower formation.

The robot-target paring method is derived from the proven auction algorithm for a single target and is extended for multi-robot multi-target cases, which optimizes effect-based robot-target pairing based on heuristic and sensory data. The multi-robot multi-target pairing method can produce a weighted attack guidance table (WAGT), which contains benefits of different robot-target pairs. The robot-target pairing converges rapidly - as is the case for auction algorithms with integer benefits.

Besides, as long as optimal robot-target pairs are obtained, a team is split into subteams formed by paired robots regarding types and numbers of the robot-target pairs with the robot-target pairing method. The subteams approach and then capture their own paired targets in the modified potential field based leader-follower formation while avoiding sensed obstacles.

Simulation studies illustrate system efficacy with the proposed control method for multi-target operations. Moreover, the paper is concluded with observations of enhanced system performance.

Keywords: Teleoperation, Multi-target Operations, and Multi-agent Systems.

1. INTRODUCTION

Cooperative control of multi-agent robotic systems has been investigated in recent years [36, 47], especially for tasks that cannot be handled by a single robot. It can improve dexterity of robots and enlarge application fields of robots. Furthermore, Fox et. al. [19] have demonstrated that multi-robots can localize themselves faster and more accurately if they exchange information about their positions whenever they sense each other. Moreover, using several low-cost robots introduces redundancy and therefore is more fault tolerant than having only one powerful and expensive robot. Therefore, there have been many cooperative control methods, e.g. the behavior based formation control, virtual structure approach, leader-follower approach, and potential field based control method for multi-robot navigation and searching [2,12,26,29,42,43].

Balch and Arkin [2] presented behavior based formation control. The temporary distortion in a formation was used to avoid obstacles. However, the system is not able to be analyzed in terms of simple mathematic equations. Therefore, exact formation control of the system cannot be guaranteed. Lalish et. al. [26] suggested the virtual structure approach by considering the robot

formation as a single virtual rigid structure. The behavior of the whole group is totally predictable, and its formation is precisely maintained. However, a wider inter-robot communication is necessary, which causes more communication delays. Desai et. al. [12] proposed a leader-follower approach. One or more robots are designated as the leader(s) and responsible for guiding the formation. The other robots are required to follow the leader(s) with predefined clearances. This leader-follower approach has some benefits, e.g. its simplicity, modularity, and reliability of the system and no need for heavy computation. However, the whole team is potentially subjected to system malfunctions if the leader(s) break(s) down. In addition, there is a risk that the followers get too close to each other while only keeping a constant leader-follower distance without considering the follower-follower distances. Due to no interconnection between the followers, the follower cannot distinguish between its team robots and obstacles. Therefore, if the robot-robot distance that the robot needs to maintain in the team is different from the robot-obstacle distance that the robot needs to keep from the obstacles, the follower may hit the other robot or obstacle. Artificial potential functions have been extensively used for multi-robot navigation and control [3,8,14,20,29,41,44]. The robots are attracted to the target while being repulsed from the obstacles as if the robots and obstacles as positive ions and the target as a negative ion were in potential fields.

By comparing those above mentioned approaches, the potential function based approaches seemed to be useful tools from the view points of flexibility of configurations of robotic teams, automatic avoidance of collisions of team robots, and stability of maintaining formations. However, the multiple fields can sum to a vector with a zero magnitude. If the robot was being attracted to a point behind the box canyon, the attractive vector would cancel the repulsive vector and the robot would remain stationary because all forces would cancel out. This is called a local minima problem [2,21,29,38,48].

Besides, all control methods discussed above for the robot cooperation are only for the fully autonomous robots. Nonetheless, the unstructured nature of the worksite environments and the limitations of the current sensors and computer decision-making technologies prohibit the use of fully autonomous systems for the operations [1,17,18,22,27,28,37]. Therefore, it is required that the human decision making be involved in the systems. Teleoperators, in which a human operator is an integral part of the control, are established to integrate the human decisions to the control loop of the systems. In order to minimize the required human resources and amplify the human effort, a single-master multi-slave (SMMS) teleoperation is considered in this paper [17,18, 22, 27, 28, 33,37].

Nevertheless, that a teleoperated robot may be of varying types with varying capabilities and limitations places significant cognitive pressure on the operator. As has been demonstrated in urban search and rescue activities [19], simply remotely operating a robotic system in a challenging environment precludes significant secondary cognitive effort (such as scanning rubble for survivors). The difficulties will be compounded when the human operator remotely guides multiple robots in a rapidly evolving operational environment. Therefore, it is required that some local robotic intelligence is added to the SMMS teleoperator to relieve human burden and enhance the performance. Nonetheless, so far a few papers have discussed the semi-autonomous SMMS teleoperation issues. Moreover, most of them were only focused on a single target operation.

However, most applications [45,46] e.g. military operation, space exploration, rescue mission, and etc, require a team of robots to form several subteams to capture multi-targets simultaneously. Therefore, the robot-target pairing method is needed to identify a proper target that can be captured by a suitable subteam of robots. Many different methods have been widely applied in fully automatic coordinated multi-robotic systems [9,11,15,30,32,35,39]. Those methods are a genetic or improved genetic [9,10,16,34], ant colony system [15,30], swarm particle optimization (SPO) [11,32], market-based approaches [13,23,24,31], and auction or decentralized cooperation auction [25,35,39]. Nonetheless, some of them [9,30,32] can have a slow convergence to the global optimum when the others [13,39] have no ability to stably

converge to a global optimum. Hence, Bogdanowicz and Coleman et. al. [4] proposed a pairing method for optimization of effect-based weapon-target pairing to decide a preferred weapon-target combination by scanning a heuristic attack guidance table. Different from those previously mentioned methods, it is a rule and function based method. Therefore, it can converge rapidly and produce a suboptimal solution stably. Nonetheless, it is derived based on some heuristic data that come from human experiences.

Due to the above mentioned problems, in this paper, the primary objective is to develop a control method for a SMMS teleoperation system to cooperatively control mobile multi-robots for a multi-target mission. Primary components of the proposed method are (1) modified potential field based leader-follower formation and (2) robot-target pairings. During the operation, the human operator only concentrates on teleoperating a team leader robot. All other team robots autonomously make a formation with regard to its positions and velocities based on sensory information. Therefore, the formation is able to be adapted by modifying their paths for obstacle avoidance and target pursuit in the modified potential field based leader-follower formation. As soon as the team is near the multi-targets, with the proposed robot-target pairing method, optimal robot-target pairs are computed, and according to them, the team is autonomously split into several subteams that are paired to appropriate targets. A subteam leader is selected based on all robot functionalities and proximity to targets to lead each subteam. Each subteam leader is able to guide all subteam robots to work on the paired targets when the subteam robots move with respect its motion.

The rest of this paper is organized as follows. In Section 2, the control method that integrates the primary components to capture multiple targets simultaneously with multiple subteams independently for is proposed. This system with the proposed control method is aimed at relieving human operator burden of teleoperating a robot team that is formed by several sub-teams in a complex environment to handle multi-targets simultaneously. In Section 3, the conditional transparency [5], i.e. the transparency if no human induced error is found, and effectiveness of the task achievement of the SMMS teleoperation system with the proposed control method were evaluated through simulation studies. Section 4 concludes this paper and shows future research directions.

2. SEMI-AUTONOMOUS TELEOPERATION CONTROL METHOD FOR A MULTI-ROBOTS-MULTI-TARGETS APPROACH

This paper proposes a control method for the semi-autonomous SMMS teleoperation to work on a multi-target mission. The major components of the control method are (1) modified potential field based leader-follower formation and (2) robot-target pairings. They are described in details in the following. During robot navigation to targets, a team/subteam moves in (1) modified potential field based leader-follower formation. Nonetheless, as long as the team is close enough to the targets, it will be split into subteams that are paired to suitable targets with (2) robot-target pairing method. Therefore, in the following, the two components are discussed and formulated in detail.

2.1 Modified Potential Field Based Leader-follower Formation

In order that the slave multi-robots can autonomously avoid the obstacles and keep a distance from other neighboring robots simultaneously while tracking the target, the approach that the most commonly has been used is potential field based formation control. Nonetheless, the potential field based formation control has the local minima problem [29], which can hold the robots in a specified formation while in motion. Therefore, the potential field based formation is modified into the one with a prioritized bonding between slave neighboring robots in this paper. The strength of the bonding between neighboring robots varies depending on which two robots are connected.

For example, the bonding between neighboring team/subteam $Leader$ and $Follower-1$ is the strongest when the one between team/subteam $Follower-n$ and $Leader$ is the weakest if there are n robots. Furthermore, as soon as the subteam is formed, only bonding between subteam

robots exists when the subteam followers move only with regard to their subteam leader. Thus, the team/subteam formation becomes adaptive due to attraction to targets and repulsion from obstacles. However, no team/subteam robot is left behind due to the robot-robot bonding with different strengths, and no subteam robot movement is affected by other subteam/team robot motion because of the elimination of the bonding between the subteam and irrelevant robots.

Besides, the team leader tracks the human commanded positions when the subteam leaders follow the reference positions to capture the targets and avoid obstacles and neighboring robots. In the potential field based leader-follower formation, all team/subteam follower paths are generated by a sum of attraction, repulsion, and prioritized bonding. All team/subteam leader paths are computed by a combination of the attraction and repulsion. In our discussion, we assume that for Robot i, the control input, u_i^i generated by using the potential field based leader-follower formation method are typically of the form.

$$u_i^i = u_a^i + u_r^i + u_b^i \tag{1}$$

where for Robot i, u_a^i is the control input caused by the attraction to the targets. u_r^i is the control input caused by the repulsion from the obstacles. u_b^i is the control input caused by the robot-robot bonding for the team/subteam followers. u_b^i can become zero for the team/subteam leaders. In the following, the control inputs due to (1) the attraction to the targets, (2) repulsion from the obstacles, and (3) bonding between robots are formulated and discussed.

2.1.1 Attraction to Targets

The control input u_a^i in Eq (1) derived from the target potential functions for the robot is formulated in Eq. (2).

$$u_a^i = \varphi_i \delta x_T \tag{2}$$

where δx_T is the sensed distance between Robot i and the paired target. Robot i can be any robot in a team or subteam. φ_i is a positive integer that becomes zero if the target is reached; otherwise, it is larger than zero. As shown in Eq. (2), if Robot i is getting closer to the paired target, u_a^i is decreased. On the contrary, if it is leaving the paired target, u_a^i is increased. Therefore, it is attracted to the paired target all the time.

2.1.2 Repulsion from Obstacles

The control input u_r^i in Eq (1) derived from the obstacle potential functions is written in Eq. (3).

$$u_r^i = \phi\langle -k_e \delta D_1 - b_e \delta V_1 \rangle \tag{3}$$

where for Robot i, $\delta V_1 = -\frac{G}{\partial x_0^2}\dot{x}_{si}$, and $\delta D_1 = -\frac{H}{\partial x_0^2}$. δx_o is the sensed robot-obstacle distance. x_{si} is the position vector of Robot i. ϕ, G, H, k_e, and b_e are positive parameters. In Eq (3), u_r^i is increased when Robot i is heading toward obstacles. On the contrary, u_r^i is decreased when it is steering away from the obstacles. Thus, it is repulsed from the obstacles all the time.

2.1.3 Bonding Between Robots

For team/subteam followers, the robot-robot bonding u_b^i in Eq. (1) is prioritized regarding the roles of the neighboring robots and formulated in the following equation.

$$u_b^i = -k_{ij}\left(r_{s\min i} - \delta x_{si}\right) \tag{4}$$

where for $i = 1.....n$ and $j = 1.....n$, $i \neq j$, k_{ij} is the positive parameter. The bonding strength varies because of different roles of the neighboring robots bonding to each other. $r_{s\min i}$ is the preferred distance that Robot i needs to keep from neighboring robots. δx_{si} is the sensed distance between Robot i and other robots. Therefore, the team/subteam followers move with regard to their team/subteam leader motion while keeping a predefined constant distance from team/subteam leader with Eq. (4) All team/subteam robots can also get around the obstacles with Eq. (3) and move toward the targets with Eq. (2)

2.2 Robot-target Pairing Method

The robot-target pairing method is sensor based and semi-distributed because all robots act largely independently in terms of planning for themselves but are able to take into account team resources by working on the tasks with other robots. It is more flexible than the centralized robot-target pairing method [9,30,32] in that each individual robot can respond to different environment stimulus independently relying on its local sensory information. In addition, it is also more robust and reliable than the distributed robot-target pairing method [13,39] in that each robot also can take advantage of sharing team resources to work with other team robots. In this paper, the team leader not only takes human commands via a master robot but also works with the robot-target pairing method as an auctioneer to send and show all bid data e.g. robot-target distances and their base prices. The bid data are also online shared by all robots, team leader and followers. All other robots, e.g. team followers, act as bidders to form a subteam by themselves in order to maximize a sum of all follower bid values and bid on the targets when the corresponding task on the targets is performed by the cooperation of the subteam. In the subteam, the bidder with the maximum bid value is selected as a subteam leader. The subteam leader is responsible for monitoring and coordinating all subteam member actions. According to the largest bid proposed by the subteam, the auctioneer, the team leader, decides which subteam wins the bid with a restriction that only one target is gained by every subteam per auction. If all subteam bid values are smaller than the base price, or any team robot cannot compute its bid value due to insufficient sensed data surrounding the targets, the auctioneer obtains the bid. If any subteam already completes the task on the target, it will inform the auctioneer to cancel the bid. The proposed robot-target pairing method is formulated and further discussed in the following.

2.2.1 Robot-target Pairing Formulation and Discussion

Consider such a scenario, in a two-dimensional and limited rectangular environment X with n_C square cells, n_p slave robots pursue n_e targets, for $n_p > n_e$. The set of the robots is denoted by a matrix of $A = \left[a_1 a_2 .....a_{n_p}\right]$ where a_{n_p} is a robot matrix of n_p. Robot Capability Vector j for Task t is denoted by $\hat{C}_j^t$, $1 \le j \le n_p$ and the set of targets is represented by a target matrix of $T = \left[T_1 T_2 .....T_{n_e}\right]$ where T_{n_e} is a target matrix of n_e. The vector representing the capability required to accomplish Task t on Target T is denoted by $\overline{C}_t^T$, $1 \le T \le n_e$. Agent $A \cup T$ denotes robot teams and targets. For simplification, we assume that both space and time can be quantized, therefore the environment can be regarded as a finite collection of cells, denoted by $X_c = [1,2....n_c]$. There exist some static obstacles with fixed sizes and regular shapes, and their locations are determined by the mapping $m : X_c \to 0,1,$ for $\forall x \in X_c, M(x) \ge thresh1$ indicates

that the cell x is occupied by obstacles. $\forall x \in X_c, M(x) \le thresh2$ indicates that the cell x is free, where $thresh2 < thresh1$ represents the threshold value between 0 and 1. Thus, each robot has different capabilities to complete different tasks on different targets.

Robot capability - For Task t and Robot j, the weighted capability vectors of Robot j can be defined as

$$\hat{C}_j^t = w_j^T diag\{b_{j1}^t b_{j2}^t ... b_{ju}^t\}[c_{j1}^t ... c_{ju}^t]^T \quad (5)$$

where u is the maximum number of the vectors, each of which represents the individual functionality. The set of robot matrices is rewritten into $A = \begin{bmatrix} a_{11}...a_{1r} \\ a_{21}...a_{2r} \\ ..... \\ a_{n_v 1}...a_{n_v r} \end{bmatrix}$ where n_v, for $0 < n_v \le n_p$, is the total number of the robots in the team, and r, for $0 < r \le n_e$ is the total number of the tasks. c_{jk}^t is a capability vector for Functionality k and Task t. w_j^T is a positive integer such that for Target T and Robot j, the following is satisfied. If the robot is assigned to the target, $w_j^T = 0$; otherwise, $w_j^T = 1$. The $u \times u$ dimension diagonal matrix of b_{ju}^t is used to estimate the percentage of possibility of using the $u \times 1$ dimensional capability vector C_j^t to do Task t by Robot j successfully. However, if Robot j does not have Capability c_{jk}^t, then b_{ju}^t is 0. Each robot matrix in A has weighted capability vectors, e.g. for Robot j and Task t, $a_{jt} = [\hat{C}_j^t]^T$.

Capability Required Executing Tasks on Targets

It is assumed that one target can be paired to two or more robots, but one robot can only be paired to one target. The capability vector that is required to accomplish Task t on Target T is defined as

$$\overline{C}_t^T = diag\{\beta_{t1}^T ....\beta_{tu}^T\} C_{tu} \quad (6)$$

where the $u \times u$ dimension diagonal matrix of β_{tu}^T is used to describe the percentage of possibility of using the $u \times 1$ dimension capability vector C_{tu} with which the robot can finish Task t on Target T. $C_{tu} = [c_{t1} ..... c_{tu}]^T$ when the total number of the vectors of the functionalities is u. c_{tu} is the capability vector that is required to complete Task t with Functionality u. However, if Task t cannot be done successfully by any robot with the capability C_{tu} on Target T, then β_{tu}^T is 0. Otherwise, β_{tu}^T is 1.

Subteam Capability

The subteam is a combination of the multi-robots that work on Task t cooperatively. For Robot j and Task t, $U_{(j,t)} = a_j e_t$ where e_t is one if Task t is assigned; otherwise, it is zero, and a_j is defined in Eq. (1) for $a_{\max} \ge j \ge a_{\min}, a_{\min} \ge 1$, and $a_{\max} \le n_p$ where $n_p / (a_{\max} - a_{\min} + 1) = n_s$ where n_s is the total number of subteams, and $a_{\max}$ and $a_{\min}$ are the

number of the first and last robots forming Subteam y, respectively. Subteam y is represented by a matrix of $D_y = \begin{bmatrix} U_{(a_{\min},1)} \ldots\ldots U_{(a_{\max},1)} \\ \ldots\ldots\ldots\ldots\ldots\ldots \\ U_{(a_{\min},r)} \ldots\ldots U_{(a_{\max},r)} \end{bmatrix}$ where r is the total number of tasks. Then, matrix A denoting a robot team formed by subteams, one of which is represented by D_y, is rewritten into $A = \{D_1 \ldots\ldots D_y \ldots\ldots D_q\}$ where q is the total number of the combinations of multi-robots (robot subteams) in the team. For Robot j and Task t, if $\hat{C}_j^t > 0$, then

$$Q_{(j,t)} = \hat{C}_j^t \qquad \text{for} \qquad n_p \geq j \geq 1 \tag{7}$$

where $Q = \{Q_{(1,t)} \ldots\ldots Q_{(n_p,t)}\}$ is a positive integer. Subteam y capability vector for Task t is defined as

$$\tilde{C}^y_{(y_a:y_b,t)} = \sum_{j=y_b}^{j=y_a} Q_{(j,t)} \tag{8}$$

where $y_b - y_a$, $\forall y_b \geq y_a$, is the total number of the robots in Subteam y. y_a is the first and y_b is the last indices of the elements in the matrix of Q for Task t and Subteam y. Subteam y is able to perform Task t on Target T if the condition, $\overline{C}_t^T \leq \tilde{C}^y_{(y_a:y_b,t)}$, is satisfied. Robot j is selected as a subteam leader when its magnitude of the capability vector $\hat{C}_j^t$ is largest in the same subteam. It is assumed that the subteam leader knows all capability information about its subteam members.

2.2.2 Bidding Winner Determination

Subteam 1	$m_{N,1}$	$\cdots$	Subteam n	$m_{N,n}$
B_1^1	$m_{1,1}$	$\cdots$	B_n^1	$m_{1,n}$
B_1^2	$m_{2,1}$	$\cdots$	B_n^2	$m_{2,n}$
$\cdots$	$\cdots$	$\cdots$	$\cdots$	$\cdots$
B_1^N	$m_{N,1}$	$\cdots$	B_n^N	$m_{N,n}$

TABLE 1: Weighted Attack Guidance Table (WAGT)

In Table 1, $m_{N,n}$ is a positive integer weight for Subteam n to bid on Target N. If $\tilde{C}^n_{(y_a:y_b,N)}$ is smaller than the base price which is a positive integer, or Target N has already been assigned to Robot Subteam n, $m_{N,n}$ is 0. Otherwise, $m_{N,n}$ is 1. By arranging $m_{N,n}$ and B_n^N into Table 1, called Weighted Attack Guidance Table (WAGT), each row of WAGT corresponds to a target and Robot Subteam (1 to n) when n is the total number of the subteams formed in the team. In addition, each column of WAGT corresponds to a robot combination (Robot Subteam) that works on Targets (1 to N) when N is the total number of the targets. Therefore, there are the N rows and n columns in WAGT. The scanning proceeds from the first to the last column. Hence, the robot combination (Robot Subteam) specified in column i takes precedence over combination of

robots specified in column $i+1$. For example, for Subteam n, Task t, and Target N, the bid value is weighted as follows.

$$B_n^N = \left(\tilde{C}^n_{(y_a:y_b,t)} - \overline{C}_t^N\right)\left(1 - X_{tn}^N\right) \tag{9}$$

where X_{tn}^N is the positive integer weight for Subteam n to do Target N. If Task t is the most preferred by Subteam n to be done on Target N when B_n^N is the maximum value of the element in the matrix of $\tilde{B}(N,n)$, then X_{tn}^N=0. Otherwise, X_{tn}^N=1. Therefore, based on the given subteams, targets, tasks, WAGT, and optimization of the robot-target pairing that is described below, the bidding winner determination is made.

The optimization of the robot-target pairing is formulated as follows. Given Subteam y, Targets N, Tasks t, and WAGT, an assignment of the subteam is found in such a format that WAGT is produced, and its corresponding objective function in Eq.(10) is maximized within the given constraints in Eqs. (11) and (12). Therefore, we can state the optimization problem as follows. For Target N and Subteam $1-n$ as seen in Table 1, the objective function is $ObjFun(N) = \left[\left(B_1^N m_{N,1}\right).....\left(B_n^N m_{N,n}\right)\right]$.

$$Maximize \qquad ObjFun(N) \tag{10}$$

Subject to

$$\sum_{y=1}^{y=n} m_{N,y} \geq 0 \tag{11}$$

$$\sum_{y=1}^{y=n} \tilde{B}(N,y) \geq 0 \tag{12}$$

where $m_{N,y}$ is defined in Table 1. Initially, all $m_{N,y}$ is equal to one if no subteam is assigned to any target. However, if Subteam y is assigned to Target N, $m_{N,y}$ is equal to zero $\forall y \;\&\; N \neq 0$. Hence, Subteam y that proposes the maximum affordable value $(B_y^N m_{N,y})$ can win Target N by solving Eqs (10) within the constraints Eqs. (11) and (12). By using the proposed robot-target pairing method, the robot-target pairs are stored into the resulted matrix e.g. a subteam-target pair matrix J_I and given WAGT. For instances, Subteam y is paired to Target N when Subteam $(y+1)$ is paired to Target $N+1$. The subteam-target pair matrix, J_I is written as $J_I = [..,N,N+1]$ when the first and second columns of the J_I represent which target is properly paired to Subteam y and $y+1$, respectively. In order to make the system be able to split its team into subteams to work on different targets simultaneously, the robot-target pairing method can also generate reference positions X_r to each subteam robot to move toward its target point by transforming J_I based on WAGT.

2.3 SMMS Teleoperator With Modified Potential Field Based Leader-follower Formation and Robot-target Pairing Methods

Figure 1 represents the overall architecture of the SMMS teleoperation system with the proposed control methods. The master and slave subsystems in Figures 1(a) and 1(b), respectively, are connected over the wireless internet. The difference from the system proposed in our papers [5] is that the slave subteam is operated fully autonomously with the modified potential field based leader-follower formation method when the team leader is teleoperated by a human operator.

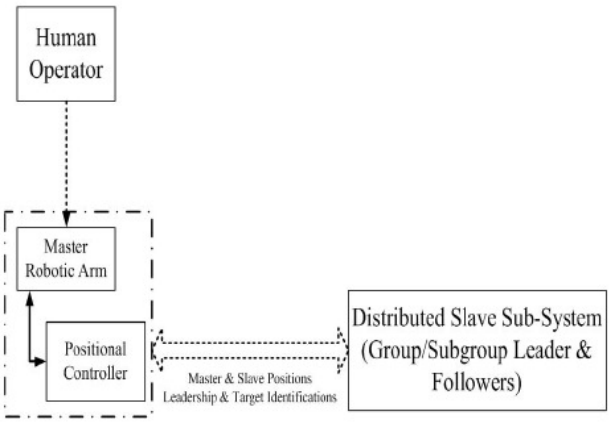

(a) Master subsystem

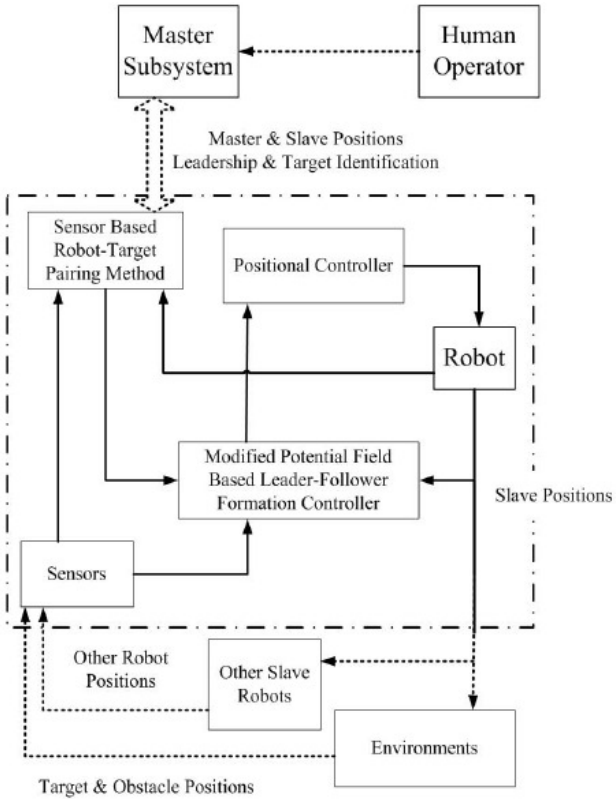

(b) Slave subsystem (leader/follower)

FIGURE 1: Modified SMMS system

In order to simplify a problem, the robot is not supposed to move so fast that the nonlinear coefficients of the robotic dynamic equation can be ignored. The proposed system shown in Figure 1 can be formulated into the following equations of motion with integration of the modified potential field based leader-follower formation and robot-target pairing methods.

Master robot:

$$M_m \ddot{e}_m + B_m \dot{e}_m + K_m e_m = 0 \tag{13}$$

Slave robot i:

$$M_{si} \ddot{e}_{si} + B_{si} \dot{e}_{si} + K_{si} e_{si} = u_a^i + u_r^i + (1-\sigma)(1-\lambda) u_b^i \tag{14}$$

where for Robot i, u_a^i, u_r^i, and u_b^i are defined in Eq (1). $e_m = x_m - x_h$, x_h and x_m are the human commanded and master sensed position vectors, respectively. $e_{si} = x_{si} - (\sigma x'_m + (1-\sigma) x'_{ideal}) x_h$, x_{si} is the position vector of the slave robot i. x'_m is the transmitted master position vector. x'_{ideal} is the reference position vector computed with respect to x'_m before a subteam is formed or X_r generated by transforming J_I resulting from Eqs (10)-(12) based on WAGT after the subteam is formed. σ is the control parameters of Robot i. When Robot i is selected as a team leader, σ is turned into one; otherwise, it becomes zero. When Robot i is appointed as a subteam leader, λ becomes one; otherwise, λ is zero. B_m is the master adaptive impedance matrix. M_m is the inertia matrix of the master robot. K_m is the control parameters for the linear diagonal master matrices. M_{si} is the inertia matrices of the slave robot i. B_{si} is the slave impedance matrix. K_{si} is the control parameters for the linear diagonal slave matrices.

By using Eqs. (13) and (14), the motion of the SMMS systems can be understood and modeled. The team moves toward a region full of multi-targets in the modified potential field based leader-follower formation when only team leader is teleoperated by the human operator via the master robot and followers autonomously move with regard to its motion. When the team is close to the targets, it can be split into subteams paired to targets with the robot-target pairing method by solving Eqs (10) within the constraints in Eqs (11) and (12). The robot-target matrix J_I is computed based on WAGT and transformed into the reference positions for the subteam robots to approach and capture the paired targets. During navigation to the paired targets, the subteams automatically move in the modified potential field based leader-follower formation again. In the formation, all subteam followers move with regard to their subteam leader's motion while the subteam leader approaches a target point computed from J_I. All subteam robots including the leader and followers can avoid obstacles while maintaining a formation. After the paired target is reached, a task, e.g. target capture, is performed by the paired subteam robots.

In the following section, the SMMS teleoperator modeled in Eqs (13) and (14) is simulated for a further study on enhancement of the performance in terms of conditional transparency [5] and task effectiveness.

3. SIMULATION STUDIES

In order to qualify and highlight the enhanced SMMS teleoperator performance, the scenario was that the SMMS system in Figure 2 with the one in [6,7] in Sim (1) and the proposed control methods in Sim (2)were properly simulated. Furthermore, Sim(1) and (2) were also subjected to the time-varying communication delay as shown in Figure 3. Results from Sim (1) and (2) are generated and compared to quantify and qualify the improvement of the performance in terms of conditional transparency [5] and task effectiveness. The simulation data from Sim (2) are discussed with findings from the research [9,13,32,39] to explicitly show advancement of convergence to an optimal solution to identify an appropriate subteam robot-target pair. The Sim (1) and (2) were set up in Table 2.

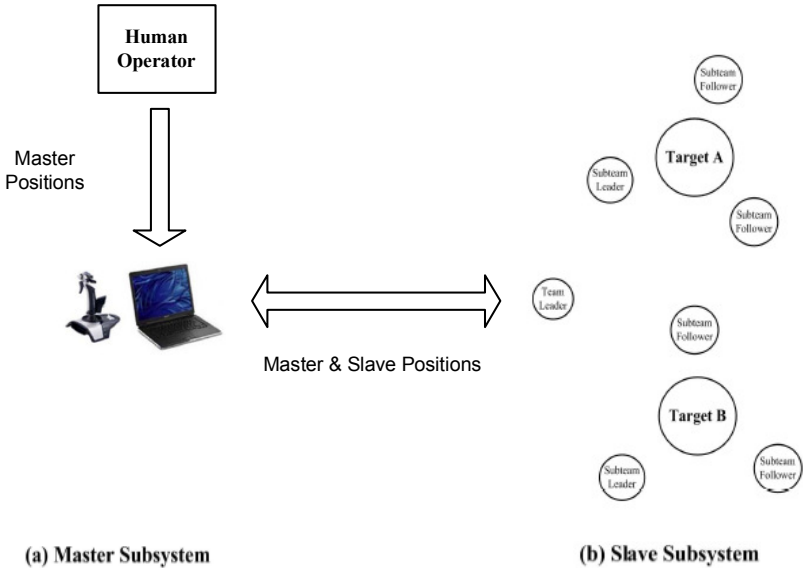

FIGURE 2: SMMS teleoperation simulation setup

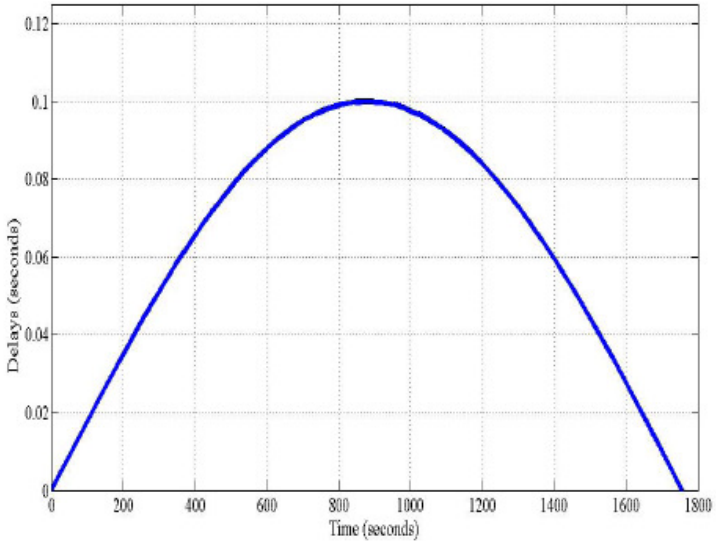

FIGURE 3: Time delays in simulations

Simulations	Control Methods	Control Objectives
Sim (1)	Positional control	adaptive leader-follower formation [7, 6]
Sim (2)	Positional control	potential field based leader-follower formation and proposed robot-target pairing

TABLE 2: SMMS simulations for a multi-target mission

In simulations, the time dependent communication delay was simulated in Figure 3. The maximum communication delay of 0.1 second was chosen in the simulations because for the earth application, there is a critical value, beyond which the system tends to become unstable

[40]. In the simulations, as shown in Figure 2, the master robot was a joystick connected to a laptop that read human operator motion commands. It was able to transmit human commands to a virtual slave robot model over the simulated TCP/IP internet. The virtual slave robots in Figure 2(b) including a team leader, subteam leaders, and followers were modeled in Matlab software and able to track the transmitted master and reference positions and velocities to execute the assigned tasks on the assigned targets. The slave robots also locally sensed the environments and then sent back the sensory information to the master robot. In the simulations, the slave robots were simulated as seven holonomic mobile platforms, each of which has two active wheels, and they formed a slave team. In addition, all of them did not have grippers. Moreover, there were six virtual static obstacles and two virtual targets in a virtual environment as shown in Figure 2. All target and robot positions were assumed to be known in the simulations, but obstacle positions were uncertain. The obstacles and targets were modeled as mass-spring-damper systems [40] in the following equations.

Targets:

$$M_T \ddot{x}_T + B_T \dot{x}_T + K_T x_T = F_T \tag{15}$$

Obstacles:

$$M_o \ddot{x}_o + B_o \dot{x}_o + K_o x_o = F_o \tag{16}$$

where M_T and M_o are the inertia matrices of the targets and obstacles, respectively. B_T and B_o are the damping coefficients of the targets and obstacles, respectively. K_T and K_o are the stiffness coefficients of the targets and obstacles, respectively. x_T and x_o are the position vectors of the targets and the obstacles, respectively. The seven slave robots were run to approach two targets, Target A (TA) and B (TB), while getting around the seven static obstacles. All targets, TA and TB, were static. The simple task, object capture, was performed by the slave robots simultaneously. Each of the targets was captured by at least three mobile robots. TA and TB were fixed on the ground. They were being captured while being encircled by the slave robots. The simulations, Sim (1) and Sim (2), as shown in Table 2, were set up with the following parameters. The desired safety distance between two robots was set to 3 m. The minimum distance between a robot and an obstacle was set to 5 m. Six circular objects with the radii of 5 m were used as obstacles in each simulation. In the simulations, the six circular obstacles, Ob1, Ob2, Ob3, Ob4, Ob5, and Ob6, were situated at (30, 60), (50, 40), (70, 20), (70,-20), (50,-40), and (30,-60), respectively. Another two circular objects with the radii of 5 m were also used as targets in each simulation. Two targets, TA and TB, were situated at (90, 30) and (90, -30), respectively, as shown in Figure 4 and 7. The seven slave robots, R1, 2, 3, 4, 5, 6, and 7, were initially located at (0, 15), (0, 10), (0, 5), (0, 0), (0, -5), (0, -10), and (0, -15), respectively. Only two directions parallel to the ground were considered in the simulations. Each slave robot was represented by a circular object with a radius of 1 m in the simulations. The master and slave positions were simulated in a computer with Matlab and divided by 10, respectively. In the simulations, the following parameters were used:

M_m = 3 kg, B_m = 6 Ns/m, K_m =6 N/m, M_{si} = 30 kg, B_{si} = 1.0 Ns/m, K_{si} = 60 N/m, M_T = 60 kg, B_T = 0.0 Ns/m, K_T = 800 N/m, M_o = 6000 kg, B_o = 0.0 Ns/m, K_o = 1000 N/m, G = H = 1, k_e = 100, b_e = 60, $r_{i\min}$ = 5, $r_{s\min}$ = 5, φ_i = ϕ = 10000, and $k_{ij} = 50000(1/i + 1/j)$

In the simulations, no friction, gravity, and air resistance were assumed in the virtual environment. The position errors are e_m and e_{si}. The simulations, Sim (1) and (2), as listed in Table 2 were conducted by the same human operator for consistency. All slave robots were programmed to move at an average speed of 0.1 m/s in the virtual environment in order to evaluate the effectiveness of the proposed systems by measuring the length of time taken to complete a task.

3.1 Simulation - Sim(1)

In Sim (1), the seven robots formed a team teleoperated by a human operator via the master robot. The human operator remotely controlled the team leader, R4, to reach TA, and all other slave robots, R1-3 and R5-7, were coordinated with R4 to surround TA to capture it. After the TA was captured, the human operator commanded R4 to move to TB while other robots, R1-3 and R5-7, were also moving with regard to R4 motion to approach TB. During the team navigations to catch TA and TB in Figure 4, all team robots were able to avoid the obstacles, Ob1-6, while they kept a constant distance from each other. As long as R4 was telecontrolled by the human operator to get to TB, R1-3 and R5-7 encircled and captured it.

In Figures 5 and 6, position errors e_{si} of the team leader and followers were presented, respectively. The position errors varied from 2.5 to 0 (m), which was caused by the time-varying communication delays. However, a position error average, 0.65 (m), was still acceptable because the team leader robot (R4) teleoperated by the human operator moved slowly when the follower robots (R1-3, 5-7) moved with regard to R4 positions. All targets were captured in 1350 seconds.

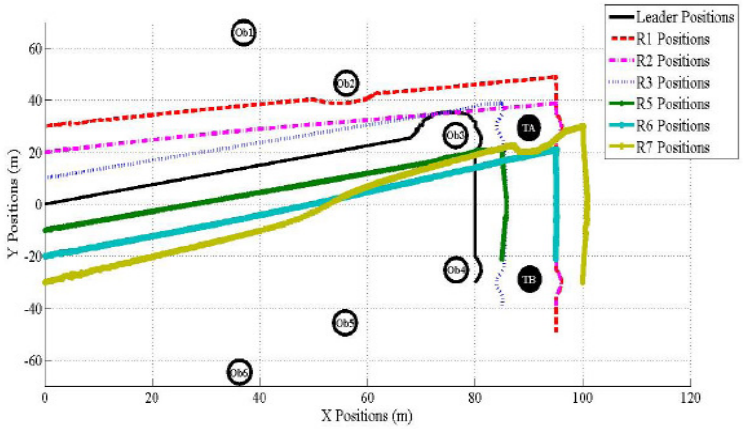

FIGURE 4: Sim(1) - Actual Path Trajectories

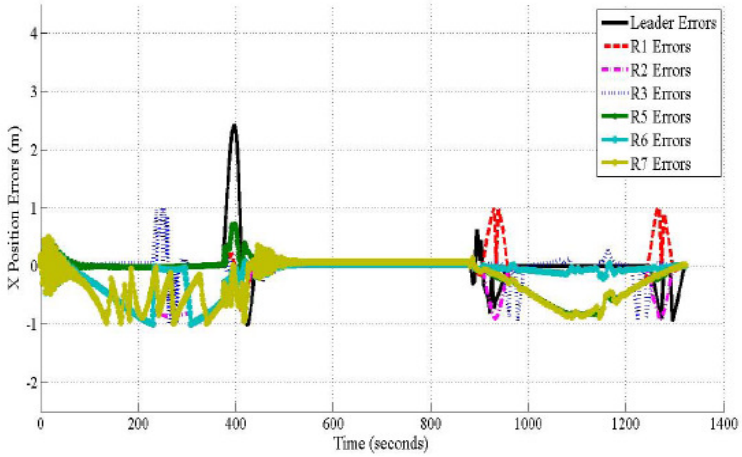

FIGURE 5: Sim(1) - Slave Positions Errors in the x-direction

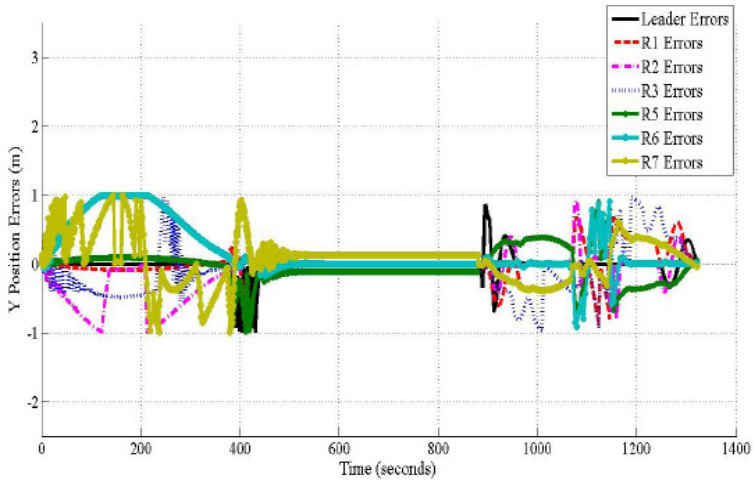

FIGURE 6: Sim(1) - Slave Positions Errors in the y-direction

3.2 Simulation - Sim(2)

In Sim (2), the task, object capture for two targets, TA and TB, was executed by the subteams formed by the seven mobile robots. The seven robots, R1-7, could form 35 types of Robot Combos (Subteams (Sub1-35)) as shown in Table 3.

Subteam	Combo	Subteam	Combo	Subteam	Combo
Sub1	R1 R2 R3	Sub13	R1 R5 R6	Sub25	R2 R6 R7
Sub2	R1 R2 R4	Sub14	R1 R5 R7	Sub26	R3 R4 R5
Sub3	R1 R2 R5	Sub15	R1 R6 R7	Sub27	R3 R4 R6
Sub4	R1 R2 R6	Sub16	R2 R3 R4	Sub28	R3 R4 R7
Sub5	R1 R2 R7	Sub17	R2 R3 R5	Sub29	R3 R5 R6
Sub6	R1 R3 R4	Sub18	R2 R3 R6	Sub30	R3 R5 R7
Sub7	R1 R3 R5	Sub19	R2 R3 R7	Sub31	R3 R6 R7
Sub8	R1 R3 R6	Sub20	R2 R4 R5	Sub32	R4 R5 R6
Sub9	R1 R3 R7	Sub21	R2 R4 R6	Sub33	R4 R5 R7
Sub10	R1 R4 R5	Sub22	R2 R4 R7	Sub34	R4 R6 R7
Sub11	R1 R4 R6	Sub23	R2 R5 R6	Sub35	R5 R6 R7
Sub12	R1 R4 R7	Sub24	R2 R5 R7		

TABLE 3: Robot combinations (robot subteams)

With the robot-target pairing method in Eqs (1) – (12), WAGT was generated. Subteams (Sub1 - 35) and their bids for the task were found for TA and TB in Table 4. Their bids were calculated in Eq. (9) as an inverse of the sum of robot-target distances in a subteam minus the base price when the base price for the task was 10. The reason was that in order to start with the tasks, the robots needed to maintain at least 10(m) from a target to capture it. The bids (T_a, T_b) in Table 4 were written where T_a was the bid values calculated for TA when T_b was the bid values calculated for TB.

Subteam	Bids	Subteam	Bids	Subteam	Bids
Sub1	(41,69)	Sub13	(39,73)	Sub25	(38,76)
Sub2	(40,69)	Sub14	(39,74)	Sub26	(39,74)
Sub3	(40,70)	Sub15	(38,75)	Sub27	(39,75)
Sub4	(40,71)	Sub16	(40,71)	Sub28	(39,75)
Sub5	(39,71)	Sub17	(40,71)	Sub29	(39,76)
Sub6	(40,70)	Sub18	(39,73)	Sub30	(38,76)
Sub7	(40,71)	Sub19	(39,73)	Sub31	(38,77)
Sub8	(40,72)	Sub20	(39,73)	Sub32	(38,77)
Sub9	(39,72)	Sub21	(39,74)	Sub33	(38,78)
Sub10	(40,72)	Sub22	(39,74)	Sub34	(38,78)
Sub11	(39,73)	Sub23	(39,75)	Sub35	(38,79)
Sub12	(39,73)	Sub24	(39,75)		

TABLE 4: Weighted Attack Guidance Table (WAGT) for Target A & B

As shown in Figure 7, only R4 was teleoperated by the human operator when all R1-3 and R5-7 automatically formed two subteams, (R1-3 and R5-7 combos) to capture TA and TB simultaneously in 625 seconds, respectively. However, R4 was not engaged in any task, which could reduce the time delay effect on the task achievements. All tasks were done by the two subteams, Sub1 and Sub35, fully autonomously. The position errors were from 0 to 0.12 (m) in Figures 8 and 9, and a position error average was 0.05 (m).

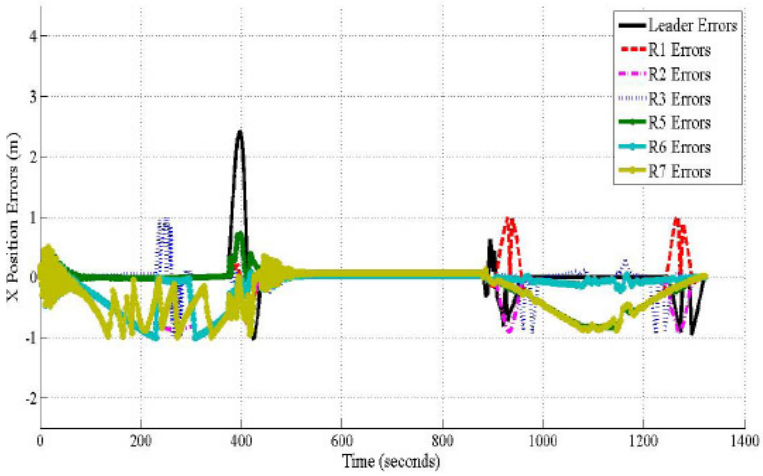

FIGURE 7: Sim(2) - Actual Path Trajectories

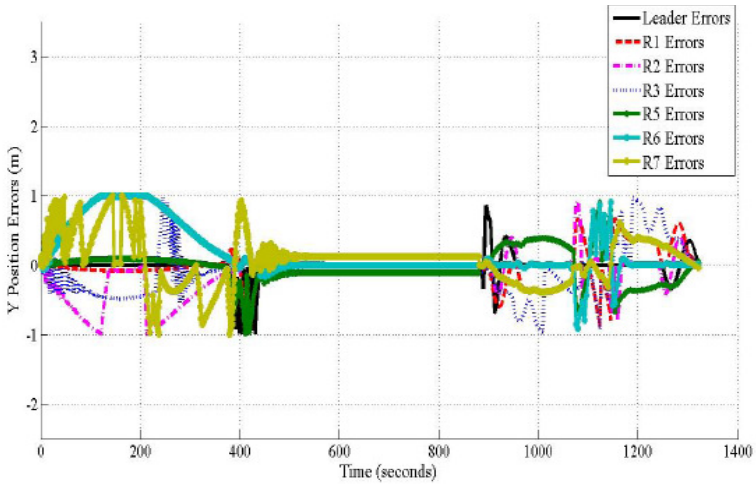

FIGURE 8: Sim(2) - Slave Positions Errors in the x-direction

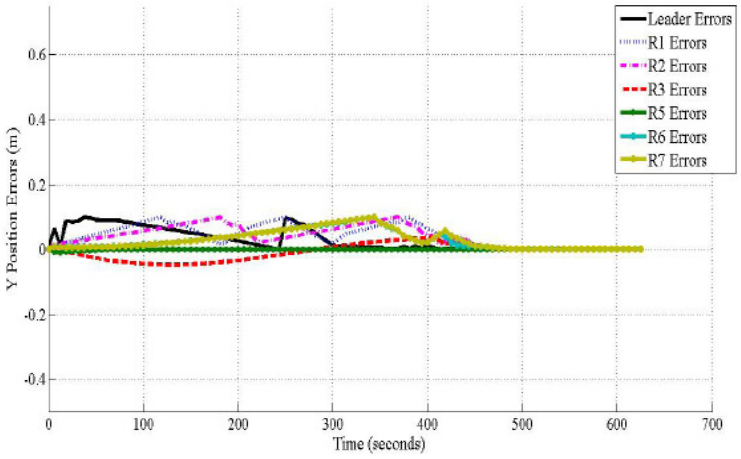

FIGURE 9: Sim(2) - Slave Positions Errors in the y-direction

3.3 Discussions on Results

Pairing methods	Execution time(seconds)	Found subteam/target pairs
Swarm particle optimization (SPO) [32]	95.6	(Sub1 - TA) and (Sub35 - TB)
Market based method [13]	103.2	(Sub1 - TA) and (Sub35 - TB)
Genetic method [9]	110.3	(Sub1 - TA) and (Sub35 - TB)
Auction based method [39]	93.2	(Sub1 - TA) and (Sub35 - TB)
Sim (2)	90.2	(Sub1 - TA) and (Sub35 - TB)

TABLE 5: Performance comparison for robot-target pairing methods

By comparing those errors in Figures 8 and 9 and 5 and 6, the performance of the system in Sim (2) was better than that in Sim (1) when the simulations showed that in Sim (2), the task was finished more quickly, and the position errors were smaller. The reasons were (1) the amount of information transmitted over the time-varying links between the master and slave subsystems became less in Sim(2) than Sim(1) when only autonomous local slave robots in Sim (2) handled the task, but the teleoperated robot, the team leader, acted as a supervisor to monitor other robot

operations. (2) Forming the subteams could save all seven robots from visiting all targets to complete the task because the seven robots were split into three robots in a subteam to perform the task on different targets simultaneously as shown in Figure 7. By taking advantage of the task planning independently done by each subteam, the task completion was more effective when the operation time was decreased to 625 seconds in Sim(2) from 1350 seconds in Sim(1) in Figures 9 and 6, respectively, since the average speeds of the robots were equivalent during the simulations.

Besides, in the simulations, we implemented different pairing methods in Table 5 to the scenario mentioned above. As shown in the table, those pairing methods were run to compute various subteam-target pairs in different durations of time so called the execution time. In comparison with the data from other findings [9,13,32,39], the convergence rates with swarm particle optimization (SPO), auction based, and proposed pairing methods [32,39] were faster than those with the market and genetic methods [9,13] by 20-30 second execution time because the algorithms for SPO, auction based, and the proposed pairing methods are simpler. However, the algorithms for the SPO and auction based methods [32,39] are rigid; hence, they are inappropriate for target capturing if an obstacle is not known beforehand, but in fact, most of the working environments in engineering applications are uncertain. Therefore, only the proposed pairing method in Sim (2) can present the relatively fast and stable convergence to get robot-target pairs because of its simple algorithm. In addition, due to its flexibility, it is also applicable to target capturing even if no apriori knowledge about obstacles is available since no obstacle data is required to solve Eqs (1) – (12).

4. CONCLUSION & FUTURE WORK

The proposed control methods are developed for the SMMS mobile teleoperations to work on multi-targets and improve the performance in terms of the effectiveness of the task achievement and the system transparency as seen from the simulation results. In the simulations, the time required to complete the task by the slave robots was reduced from 1350 seconds in Sim (1) to 625 seconds in Sim (2). With the proposed robot-target pairing method, the robots made subteams that autonomously worked on paired targets in the modified potential field leader-follower formation, which makes the SMMS system be capable of handling multi-targets simultaneously in a short time. Moreover, by comparing the proposed robot-target pairing method to the others in [9,30,32,39], it is so simple that a relatively fast convergence rate to obtain an optimal solution (proper robot-target pairs) is achieved. Besides, the results also showed that the smaller position errors in Sim(2) than those in Sim(1) represents the transparency enhancement. The reason is the effect on the robotic system due to the time-varying communication delays is reduced because during the operation, with the proposed control methods, all slave robots except a team leader become completely autonomous. The team leader is the only robot teleoperated by the human operator in a team but not engaged in any task when the time-varying delays mostly happen over the long distance wireless communication between the master and slave team leader robots [28,27]. Therefore, it was shown that in Sim (2), task efficiency and conditional transparency were improved despite the fact that the system was subjected to the time-varying communication delay. Moreover, the slave robots with the proposed control methods can avoid obstacles and track and then capture targets when (1) the modified potential field based leader-follower formation and (2) the robot-target pairing method take effect. Nonetheless, the robot-target pairing method could only generate a suboptimal solution in general since it is based on some heuristic data that come from human experiences.

Therefore, our future work will be to further evaluate the performance of the MRMTMT pairing method and the performance and quality of the robot-target pair solutions. In addition, we will look into the proposed control method for a SMMS system working in very complex tasks and environments, e.g. a task that may require identification of positions and types of the uncertain targets in an unknown area. We will install the proposed control methods into SMMS system hardware for further experimental validation based on comparative studies on the results from experiments and simulations to emphasize the expected good performance achievement although the real time delays may vary irregularly.

5. REFERENCES

[1] K. R. Baghaei and A. Agah. "task allocation methodologies for multi-robot systems", *Technical Report ITTC-FY2003-TR-20272-01*, 2003.

[2] T. Balch and R.C. Arkin. "behavior-based formation control for multirobot teams", *Robotics and Automation, IEEE transactions*, 14(6):926-939, 1998.

[3] L. Barnes, W. Alvis, M.A. Fields, K. Valavanis, and W. Moreno. "heterogeneous swarm formation control using bivariate normal functions to generate potential fields", *Distributed Intelligent Systems: Collective Intelligence and Its Applications, 2006. DIS 2006, IEEE Workshop*, pages 85-94, 2006.

[4] Z. R. Bogdanowicz and N.P. Coleman. "new algorithm for optimization of effect-based weapon-target pairings", *International Conference Scientific Computing CSC 08*, 2008.

[5] Y. Cheung. "Adaptive semi-autonomous teleoperation of a mutli-agent robotic system", *PhD thesis,* Stevens Institute of Technology, 2009.

[6] Y. Cheung and J. Chung. "cooperative control of a multi-arm system using semi-autonomous telemanipuation and adaptive impedance", *14th IEEE International Conference on Advanced Robotics (ICAR)*, 2009.

[7] Y. Cheung, J.H. Chung, and N. Coleman, "semi-autonomous formation control of a single-master multi-slave teleoperation system"*, IEEE Symposium on Computational Intelligence in Control and Automation*, 2009.

[8] S. Cifuentes, J.M. Giron-Sierra, and J.F. Jimenez, "robot formation control based on a multi-potential approach", *Control Automation and Systems (ICCAS), 2010 International Conference*, pages 1982-1987, 2010.

[9] L. Delin, S. Chunlin, W. Biao, and W. Wenhai, "air combat decision-making for cooperative multiple target attack using heuristic adaptive genetic algorithm", *Machine Learning and Cybernetics, Proceeding of 2005 International Conference*, (1)473-478, 2005.

[10] L. Delin, D. Haibin, W. Shunxiang, and L. Maoqing, "research on air combat decision-making for cooperative multiple target attack using heuristic ant colony algorithm", *ACTA AERONAUTICA ET ASTRONAUTICA SINICA*, 27(6) pages 1166-1170, 2006.

[11] L. Delin, Y. Zhong, D. Haibin, W. Zaigui, and S. Chunlin, "heuristic particle swarm optimization algorithm for air combat decision-making on CMTA", *Transactions of Nanjing University of Aeronautics and Astonautics*, 23(1) pages. 20-26, 2006.

[12] J.P. Desai, J.P. Ostrowski, and V. Kumar, "modeling and control of formations of non-holonomic mobile robots", *Robotics and Autonmation, IEEE Transactions*, 17(6) pages. 905-908, 2001.

[13] M.B. Dias, R.M. Zlot, N. Kalra, and A. Stentz, "market-based multirobot coordination: a survey and analysis", *Proceedings of the IEEE*, 94(7) pages. 1257-1270, 2006.

[14] K.D. Do, "formation control of mobile agents using local potential functions*", American Control Conference*, 2006.

[15] M. Eghbali and M.A. Sharbafi, "multi-agent routing to multi-targets via ant colony", *Computer and Automation Engineering (ICCAE), 2010 the 2nd International Conference*, (1)pages. 587-591, 2010.

[16] P.G. Espejo, S. Ventura, and F. Herrera, "a survey on the application of genetic programming to classification", *Systems, Man., and Cyberetics, Part C: Applications and Reviews, IEEE Transactions*, 40(2), pages. 121-144, 2010.

[17] I. Farkhatdinov and J.H. Ryu, "teleoperation of multi-robot and multi-property systems", *Industrial Informatics, INDIN 2008, 6th IEEE International Conference*, pages 1453-1458, 2008.

[18] T. Fong, C. Thorpe, and C. Baur, "multi-robot remote driving with collaborative control", *Industrial Electronics, IEEE Transactions*, 50(4) pages. 699-704, 2003.

[19] D. Fox, W.Burgard, H. Kruppa, and S. Thrun, "collaborative multi-robot localization", *In Proceedings of the German Conference on Artificial Intelligence and the 21st Symposium on Pattern Recognition*, 1999.

[20] S.S. Ge, C.H. Fua, and W.M. Liew, "swarm formations using the general formation potential function", *Robotics, Automation, and Mechatronics, 2004 IEEE Conference*, (2) pages. 655-660, 2004.

[21] J.P. Graciano, "a simple navigation algorithm with no local minima", *Advanced Robotics, ICAR 2005, Proceedings, 12th International Conference,* pages 640-646, 2005.

[22] K. Hashtrudi-Zaad and S.E. Salcudean, "adaptive transparent impedance reflecting teleoperation", *Proceeding of the 1996 IEEE International Conference on Robotics and Automation,* 1996.

[23] B. Kaleci, O. Parlaktuna, M. Ozkan, and G. Kirlik, "market-based task allocation by using assignment problem", *Systems, Man, and Cybernetics (SMC), 2010, IEEE International Conference*, pages 135-141, 2010.

[24] M.T. Khan, T. Imanuel, and C.W. DeSilva, "autonomous market-based multi-robot cooperation", *Intelligent and Advanced Systems (ICIAS), 2010 International Conference*, pages 1-6, 2010.

[25] W. Kim, D.S. Cho, and H.J. Kim, "sequential multi-agent task assignment using auction algorithm based on d*lite", *Control Automation and Systems (ICCAS), 2010 International Conference,* page 938-942, 2010.

[26] E. Lalish, K.A. Morgansen, and T. Tsukamaki, "formation tracking control using virtual structures and deconfliction", *Decision and Control, 2006, 45th IEEE Conference*, pages 5699-5705, 2006.

[27] D. Lee, O. Martinez-Palafox, and M.W. Spong, "bilateral teleoperation of multiple cooperative robots over delayed communication networks: Theory", *Robotics and Automation, ICRA, Proceedings of the IEEE International Conference*, 2005.

[28] D. Lee and M.W. Spong, "bilateral teleoperation of multiple cooperative robots over delayed communication networks: Application", *Robotics and Automation, ICRA Proceedings of the 2005 IEEE International Conference,* 2005.

[29] H.K. Lee, M.H. Shin, and M.J. Chung, "adaptive controller of master-slave systems for transparent teleoperation", *ICAR 1997*, pages 14-23, 1997.

[30] Z.J. Lee, C.Y. Lee, and S.F. Su, "an immunity-based ant colony optimization algorithm for solving weapon target assignment problem", *Applied Soft Computing Journal,* 2(1) pages. 39-47, 2002.

[31] C.S. Lim, R. Mamat, and T. Braunl, "market-based approach for multi-team robot cooperation", *Autonomous Robots and Agents, 2009, ICARA 2009, 4th International Conference,* pages 62-67, 2009.

[32] B. Liu, Z. Qin, R. Wang, Y.B. Gao, and L.P. Shao, "a hybrid heuristic particle swarm optimization for coordinated multi-target assignment", *Industrial Electronics and Applications, ICIEA, 4th IEEE Conference,* pages 1929-1934, 2009.

[33] J. Liu, L. Shun, T. Chen, X. Huang, and C. Zhao, "competitive multi-robot teleoperation", Robotics and Automation, 2005, ICRA 2005, *Proceedings of the 2005 IEEE International Conference,* pages 75-80, 1993.

[34] K.F. Man, F.S. Tang, and S. Kwong, "genetic algorithms: concepts and applications in engineering designs", *Industrial Electronics, IEEE Transactions*, 43(5) pages. 519-534, 1996.

[35] S. Monteiro and E. Bicho, "robots allocation and leader-follower pairs", *Robotics and Automation, ICRA, IEEE International Conference*, pages 3769-3775, 2008.

[36] J. Ota, N. Miyata, T. Arai, E. Yoshida, D. Kurabatashi, and J. Sasaki, "transferring and regrasping a large object by cooperation of multiple mobile robots", *Human Robot Interaction and Cooperative Robots, Proceedings of IEEE/RSJ International Conference*, 1995.

[37] H. Park, Y.A. Lim, A. Pervez, B.C. Lee, S.G. Lee, and J. Ryu, "teleoperation of a multi-purpose robot over the internet using augumented reality*", Control, Automation, and Systems, 2007, ICCAS 2007, International Conference*, pages 2456-2461, 2007.

[38] M.G. Park and M.C. Lee, "real-time path planning in unknown environment and a virtual hill concept to escape local minima", *Industrial Electronics Society, 2004, IECON 2004, 30th Annual Conference of IEEE,* (3) pages.2223 – 2228, 2004.

[39] A. Pongpunwattana and R. Rysdyk, "real-time planning for multiple autonomous vehicles in dynamic uncertain environments", *Journal of Aerospace Computing, Information, and Communication*, 1(12) pages. 580-604, 2004.

[40] J.H. Ryu, D.S. Kwon, and B. Hannaford, "stable teleoperation with time-domain passivity control", *Robotics and Automation, IEEE Transactions*, 20(2) pages. 365-373, 2004.

[41] C. Sabattini, C. Secchi, and C. Fantuzzi, "potential based control strategy for arbitrary shape formations of mobile robots", *Intelligent Robots and Systems, 2009, IROS 2009, IEEE/RSJ International Conference,* pages 3762-3767, 2009.

[42] T. Suzuki, T. Sekine, T. Fujii, H. Asama, and I. Endo, "cooperative formation among multiple mobile robot teleoperation in inspection task", *Decision and Control 2000, Proceedings of the 39th IEEE Conference*, 1(12-15), pages. 358-363, 2000.

[43] H. Tan, Q. Liao, and J. Zhang, "an improved algorithm of multiple robot cooperation in obstacle existing environment", *Robotics and Biomimetics, 2007, ROBIO 2007*, pages 1001-1006, 2007.

[44] L.M. Wachter and L.E. Ray, "stability of potential function formation control with communication and processing delay", *American Control Conference, 2009, ACC 2009*, pages 2997-3004, 2009.

[45] Z. Wang, M.N. Admadabadi, E. Nakano, and T. Takahashi, "a multiple robot system for cooperative object transportation with various requirements on task performing", *Robotics and Automation, 1999, Proceedings of 1999 IEEE International Conference*, 2(10-15) pages 1226-1233, 1999.

[46] H. Yamaguchi, "a distributed motion coordination strategy for multiple nonholonomic mobile robots in cooperative hunting operations", Decision and Control, 2002, Proceedings of the 41st IEEE Conference, 3(10-13) pages 2984-2991, 2002.

[47] Y. Yamamoto and S. Fukuda, "trajectory planning of multiple mobile manipulators with collision avoidance capability", *Proceedings of ICRA 2002 IEEE International Conference*, 2002.

[48] Z. Yao and K. Gupta, "distributed strategies for local minima escape in motion planning for mobile networks", *Robot Communication and Coordination, 2009, ROBO-COMM 2009, Second International Conference*, pages 1-7, 2009.

INSTRUCTIONS TO CONTRIBUTORS

Robots are becoming part of people's everyday social lives - and will increasingly become so. In future years, robots may become caretaking assistants for the elderly, or academic tutors for our children, or medical assistants, day care assistants, or psychological counselors. Robots may become our co-workers in factories and offices, or maids in our homes.

The International Journal of Robotics and Automation (IJRA), a refereed journal aims in providing a platform to researchers, scientists, engineers and practitioners throughout the world to publish the latest achievement, future challenges and exciting applications of intelligent and autonomous robots. IJRA is aiming to push the frontier of robotics into a new dimension, in which motion and intelligence play equally important roles. IJRA scope includes systems, dynamics, control, simulation, automation engineering, robotics programming, software and hardware designing for robots, artificial intelligence in robotics and automation, industrial robots, automation, manufacturing, and social implications.

To build its International reputation, we are disseminating the publication information through Google Books, Google Scholar, Directory of Open Access Journals (DOAJ), Open J Gate, ScientificCommons, Docstoc and many more. Our International Editors are working on establishing ISI listing and a good impact factor for IJRA.

The initial efforts helped to shape the editorial policy and to sharpen the focus of the journal. Starting with volume 2, 2011, IJRA appears in more focused issues. Besides normal publications, IJRA intend to organized special issues on more focused topics. Each special issue will have a designated editor (editors) – either member of the editorial board or another recognized specialist in the respective field.

We are open to contributions, proposals for any topic as well as for editors and reviewers. We understand that it is through the effort of volunteers that CSC Journals continues to grow and flourish.

IJRA LIST OF TOPICS

The realm of International Journal of Robotics and Automation (IJRA) extends, but not limited, to the following:

- Automation Control
- Autonomous Robots
- Emergence of The Thinking Machine
- Household Robots and Automation
- Jacobian and Singularities
- Nanotechnology & Robotics (Nanobots)
- Robot Controller
- Robotic & Automation Software Development
- Robotic Surgery
- Robotic Welding
- Robotics Programming
- Robots Society and Ethics
- Spatial Transformations
- Unmanned (Robotic) Vehicles
- Automation Engineering
- Biotechnology & Robotics
- Forward Kinematics
- Inverse Kinematics
- Methods for Teaching Robots
- Orientation Matrices
- Robot Structure and Workspace
- Robotic Exploration
- Robotic Surgical Procedures
- Robotics Applications
- Robotics Technologies
- Software and Hardware Designing for Robots
- Trajectory Generation

CALL FOR PAPERS

Volume: 2 - **Issue:** 4 - July 2011

i. Paper Submission: July 31, 2011 **ii. Author Notification:** September 01, 2011

iii. Issue Publication: September / October 2011

CONTACT INFORMATION

Computer Science Journals Sdn BhD
M-3-19, Plaza Damas Sri Hartamas
50480, Kuala Lumpur MALAYSIA

Phone: 006 03 6207 1607
006 03 2782 6991

Fax: 006 03 6207 1697

Email: cscpress@cscjournals.org

INSTRUCTIONS TO CONTRIBUTORS

Robots are becoming part of people's everyday social lives - and will increasingly become so. In future years, robots may become caretaking assistants for the elderly, or academic tutors for our children, or medical assistants, day care assistants, or psychological counselors. Robots may become our co-workers in factories and offices, or maids in our homes.

The International Journal of Robotics and Automation (IJRA), a refereed journal aims in providing a platform to researchers, scientists, engineers and practitioners throughout the world to publish the latest achievement, future challenges and exciting applications of intelligent and autonomous robots. IJRA is aiming to push the frontier of robotics into a new dimension, in which motion and intelligence play equally important roles. IJRA scope includes systems, dynamics, control, simulation, automation engineering, robotics programming, software and hardware designing for robots, artificial intelligence in robotics and automation, industrial robots, automation, manufacturing, and social implications.

To build its International reputation, we are disseminating the publication information through Google Books, Google Scholar, Directory of Open Access Journals (DOAJ), Open J Gate, ScientificCommons, Docstoc and many more. Our International Editors are working on establishing ISI listing and a good impact factor for IJRA.

The initial efforts helped to shape the editorial policy and to sharpen the focus of the journal. Starting with volume 2, 2011, IJRA appears in more focused issues. Besides normal publications, IJRA intend to organized special issues on more focused topics. Each special issue will have a designated editor (editors) – either member of the editorial board or another recognized specialist in the respective field.

We are open to contributions, proposals for any topic as well as for editors and reviewers. We understand that it is through the effort of volunteers that CSC Journals continues to grow and flourish.

IJRA LIST OF TOPICS

The realm of International Journal of Robotics and Automation (IJRA) extends, but not limited, to the following:

- Automation Control
- Autonomous Robots
- Emergence of The Thinking Machine
- Household Robots and Automation
- Jacobian and Singularities
- Nanotechnology & Robotics (Nanobots)
- Robot Controller
- Robotic & Automation Software Development
- Robotic Surgery
- Robotic Welding
- Robotics Programming
- Robots Society and Ethics
- Spatial Transformations
- Unmanned (Robotic) Vehicles
- Automation Engineering
- Biotechnology & Robotics
- Forward Kinematics
- Inverse Kinematics
- Methods for Teaching Robots
- Orientation Matrices
- Robot Structure and Workspace
- Robotic Exploration
- Robotic Surgical Procedures
- Robotics Applications
- Robotics Technologies
- Software and Hardware Designing for Robots
- Trajectory Generation

CALL FOR PAPERS

Volume: 2 - **Issue:** 4 - July 2011

i. Paper Submission: July 31, 2011 **ii. Author Notification:** September 01, 2011

iii. Issue Publication: September / October 2011

CONTACT INFORMATION

Computer Science Journals Sdn BhD
M-3-19, Plaza Damas Sri Hartamas
50480, Kuala Lumpur MALAYSIA

Phone: 006 03 6207 1607
006 03 2782 6991

Fax: 006 03 6207 1697

Email: cscpress@cscjournals.org